CHALMERS
UNIVERSITY OF TECHNOLOGY

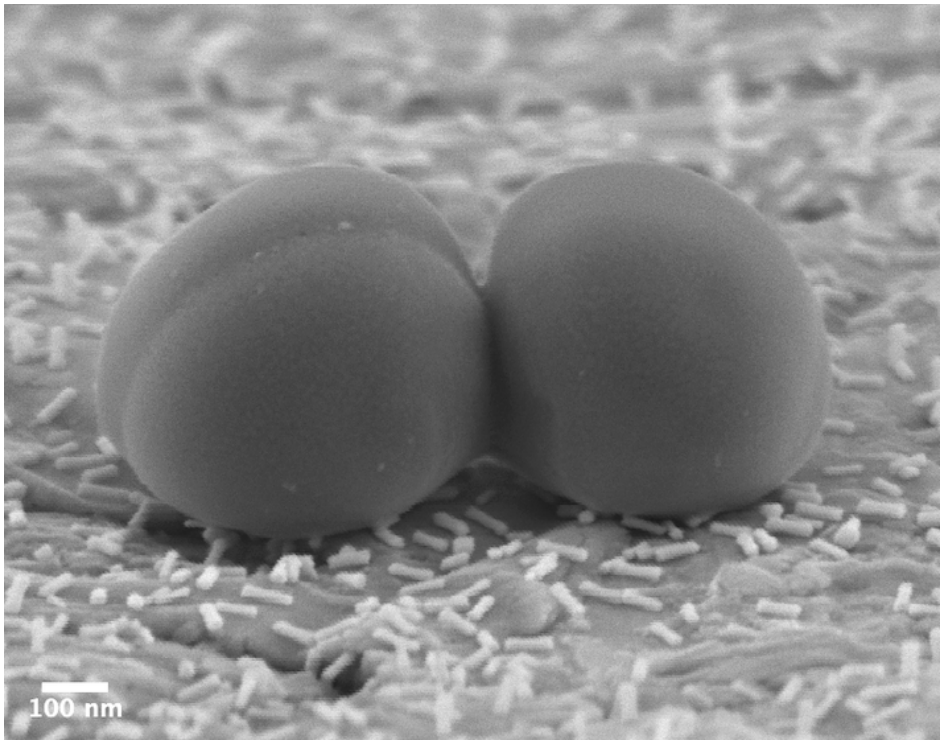

Gold Nanorod-Functionalised Surfaces for the Photothermal Elimination of Bacteria

Using localised surface plasmon resonance-generated heat to fight implant-associated infections

Master's thesis in Materials Chemistry

Maja Uusitalo

Department of Chemistry and Chemical Engineering
CHALMERS UNIVERSITY OF TECHNOLOGY
Gothenburg, Sweden 2021

Master's thesis 2021: KBTX61

Gold Nanorod-Functionalised Surfaces for the Photothermal Elimination of Bacteria

Using localised surface plasmon resonance-generated heat to fight implant-associated infections

Maja Uusitalo

CHALMERS
UNIVERSITY OF TECHNOLOGY

Department of Chemistry and Chemical Engineering
Division of Applied Chemistry
M. A. Research Group
Chalmers University of Technology
Gothenburg, Sweden 2021

Gold Nanorod-Functionalised Surfaces for the Photothermal Elimination of Bacteria
Using localised surface plasmon resonance-generated heat to fight implant-associated infections
Maja Uusitalo

Supervisor: Mats Hulander, Department of Chemistry and Chemical Engineering
Examiner: Martin Andersson, Department of Chemistry and Chemical Engineering

Master's Thesis 2021:KBTX61
Department of Chemistry and Chemical Engineering
Division of Applied Chemistry
M. A. Research Group
Chalmers University of Technology
SE-412 96 Gothenburg
Telephone +46 31 772 1000

Cover: SEM micrograph at 150 000x magnification of *S. epidermidis* on gold nanorod-functionalised titanium.

Typeset in LaTeX
Printed by Chalmers Reproservice
Gothenburg, Sweden 2021

Gold Nanorod-Functionalised Surfaces for the Photothermal Elimination of Bacteria
Using localised surface plasmon resonance-generated heat to fight implant-associated infections

Maja Uusitalo
Department of Chemistry and Chemical Engineering
Chalmers University of Technology

Abstract

Implant-associated infections constitute a significant limitation to the use of medical implants, and the development of alternatives to conventional antibiotics for prevention and/or treatment of these infections would have a great impact on the future use of medical implants. In this thesis, a strategy for utilising gold nanorod-functionalised surfaces that are irradiated with near-infrared (NIR) light in order to photothermally eliminate bacteria from the surfaces has been developed and evaluated. Gold nanorods were synthesised through a seed-mediated synthesis procedure, and subsequently surface assembled onto titanium and glass substrates via chemisorption using (3-mercaptopropyl)trimethoxysilane as a linker.

The antimicrobial activity of the gold nanorod-functionalised surfaces upon irradiation with near-infrared light was evaluated through *in vitro* studies with *Staphylococcus epidermidis* as a representative bacterial species commonly causing implant-associated infections. From the *in vitro* study performed with the gold nanorod-functionalised glass an evident antimicrobial activity was observed, where the gold nanorod-functionalised glass irradiated with NIR light exhibited 40-50% more dead bacteria than the control groups. The results highlight that the principle of using surface assembled gold nanorods to photothermally eliminate bacteria upon irradiation with NIR light is a possible alternative to conventional antibiotics in the fight against implant-associated infections. No evident antimicrobial activity could be observed from the *in vitro* studies performed with the gold nanorod-functionalised titanium upon exposure to NIR light. The lack of antimicrobial activity was attributed to two main factors; a red-shift occurring in the localised surface plasmon resonance frequency of the gold nanorods due to changes in refractive index of the local environment arising once assembled on titanium, and the titanium substrate having a plasmon damping effect on the gold nanorods. Based on the results from all the *in vitro* studies performed during the project, no apparent toxic effect of the gold nanorods themselves could be noticed, showing promise for potential future biological applications.

Keywords: Implant-associated infections, gold nanorods, localised surface plasmon resonance, surface functionalisation, antimicrobial surfaces

Acknowledgements

I would like to thank my examiner Martin Andersson for the opportunity to work with this master's thesis, as well as for the support and enthusiasm you have showed throughout the project. I would also like to express my gratitude to my supervisor Mats Hulander. Thank you for your encouragement, and for always being willing to help and answer my endless stream of questions. In addition, a big thank you to Edvin Blomstrand and Annija Stepulane for helping me with the microbiology work in my project. To the rest of the members of M. A. Research Group, thank you for welcoming me and making working in the lab together such an enjoyable experience. Furthermore, I want to thank Marika Gugole for all the help and the fresh ideas you have contributed with during the project.

Lastly, I would like to thank my family and friends for their support.

Maja Uusitalo, Gothenburg, April 2021

Contents

List of Figures

List of Tables

1

Introduction

Implant-associated infections are a serious ongoing problem in today's society and constitute a considerable limitation to the use of medical implants. Infections associated with surgical implants are generally hard to manage as they demand long periods of antibiotic treatment and sometimes repeated surgical procedures [1], leading to both clinical and economical implications. Furthermore, the demand for medical implants will only become greater with the increase in life expectancy and the progress of medical technology [2]. Despite the technological progress made, implant-associated infections remain one of the most frequent and serious complications related to the use of biomaterials [3], with no apparent improvement observed in the infection rates. The prevention and/or treatment of implant-associated infections is thus a critical matter that could have a great impact on the future use of medical implants.

Bacterial adhesion to an implant surface and subsequent formation of a biofilm, that is, bacteria enclosed in a biopolymer matrix, is the origin of implant-associated infections and one of the main reasons for removal of medical implants [2]. The biopolymer matrix of a biofilm is self-produced by the bacteria and provide both protection and structural support. Biofilm-growing bacteria exhibit a much higher tolerance to antibiotics, up to 1000-fold higher concentrations compared to planktonic bacteria [4], making the treatment of implant-associated infections a considerable challenge. Together with the currently emerging problem of antimicrobial resistance [5], the difficulties related to the treatment makes the development of alternative ways of fighting implant-associated bacterial infections a highly relevant topic.

A possible alternative to conventional antibiotics for the prevention or treatment of implant-associated infections is the use of gold nanorods in combination with near-infrared light to photothermally eliminate bacteria. The irradiation of gold nanorods, with light of their plasmon resonance frequency, leads to absorption and subsequent excitation of conduction band electrons. The excitation of conduction band electrons results in coherent oscillations of the electrons along the gold nanorod surface, which are known as localised surface plasmons. When the localised surface plasmons decay their energy is transferred to the local surroundings as heat [6]. If gold nanorods are attached to a substrate surface and subsequently irradiated with light of their plasmon resonance frequency, leading to the generation of localised surface plasmons, the local heating arising from the decay of the plasmons can be used to photothermally eliminate bacteria from the surface. Furthermore, the localised surface plasmon resonance frequency of gold nanorods can be adjusted by changing the dimensions of the nanorods. The strong absorption from the gold nanorods can thus be tuned

into the near-infrared frequency region around 750-1500 nm, where aqueous tissue absorbs the minimum amount of light [6]. By utilising gold nanorods that absorb in the near-infrared region it could therefore be possible to externally activate the antimicrobial activity of the surfaces. The possibility of tuning the absorption of the gold nanorods, and thereby control where the localised surface plasmon resonance occurs, thus make them suitable for clinical therapy applications.

1.1 Purpose and objectives

The purpose of the thesis is to develop and evaluate a strategy for utilising gold nanorod-functionalised surfaces that are irradiated with near-infrared light to photothermally eliminate bacteria from the surfaces. The objectives include the synthesis of gold nanorods with a localised surface plasmon resonance frequency in the near-infrared region, and the subsequent surface assembly of the nanorods on glass and titanium substrates. The gold nanorod-functionalised surfaces should exhibit an even coverage of gold nanorods without any larger aggregates of nanorods formed. To achieve these surface properties, a surface assembly procedure will be developed wherein the gold nanorods are chemisorbed onto the substrates via an organosilane linker molecule. The objectives further include the evaluation of the antimicrobial activity of the gold nanorod-functionalised surfaces upon irradiation with near-infrared light through *in vitro* studies.

1.2 Limitations

Gold nanorods will solely be synthesised through a wet chemical, seed-mediated synthesis procedure utilising hexadecyltrimethylammonium bromide (CTAB) as a capping agent. Gold nanorods stabilised by other capping agents, such as citrate, will not be evaluated. The substrates that will be assessed for the gold nanorod-functionalised surfaces in the project will be limited to glass and titanium. Glass substrates will be utilised as previous work has been done on gold nanorod-functionalised glass, showing that it is possible to achieve the desired photothermal elimination of bacteria upon irradiation with near-infrared light [7]. Titanium substrates will be evaluated as titanium and different titanium alloys are common materials used for medical implants and thus make a good representative material for the intended application.

For the evaluation of the antimicrobial activity of the gold nanorod-functionalised surfaces, the bacterial species used will be limited to *Staphylococcus epidermidis* as a representative species commonly causing implant-associated infections. Furthermore, the antimicrobial activity will only be assessed through *in vitro* studies. Consequently, no actual implantation and *in vivo* studies using animal models will be conducted during the project.

2

Theory

2.1 Implant-associated infections

Implant-associated infections are caused by bacterial adhesion to the surface of a biomaterial. Infections related to medical implants commonly originate from microbial contamination during the surgical procedure, and at the time of implantation there is a competition between integration of the surrounding tissue with the implant and bacterial adhesion to the implant surface [2]. The competition between the host cells and bacteria to occupy the surface of the implant is crucial for successful implantation and is often described as the concept of "race for the surface" [3]. If bacterial adhesion occurs and bacterial growth is initiated, over time some bacterial species may form biofilms on the implant surface. A bacterial biofilm consists of bacterial aggregates that are enclosed in a biopolymer matrix made out of extracellular polymeric substances produced by the bacteria. Biofilm-growing bacteria are protected from the immune response by the surrounding biopolymer matrix and also exhibit a greatly increased resistance to antibiotics and other conventional antimicrobial therapies [2]. Implant-associated infections caused by biofilm-growing bacteria are, due to the increased resilience towards both the immune response and antimicrobial therapies, often very difficult to treat and as a result, removal of implants is becoming more prevalent [2]. Infections related to implants thereby constitute a considerable limitation to the use of medical implants.

2.1.1 Pathogens causing implant-associated infections

The most common bacterial species that cause implant-associated infections include *Staphylococcus aureus* and *Staphylococcus epidermidis* [2]. Both *S. aureus* and *S. epidermidis* are biofilm-forming, Gram-positive bacteria that can be found on human skin, but while *S. aureus* only colonises a certain percentage of healthy human adults, *S. epidermidis* make up a part of the normal human skin flora. Implant-associated infections caused by *S. aureus* commonly proceed more rapidly and are more severe, while *S. epidermidis* has greater accessibility as an opportunistic pathogen due to being a permanent coloniser of human skin. Other pathogens causing implant-associated infections include the Gram-negative bacteria *Pseudomonas aeruginosa* and *Escherichia coli* [2].

2.1.2 Antimicrobial resistance

Further complicating the problem with implant-associated infections is the issue of antimicrobial resistance. Antimicrobial resistance is the capability of a microorganism to resist the mechanism of action of an antimicrobial agent, such as antibiotics, and constitute a growing problem in today's society [5]. Antimicrobial resistance in bacteria is caused by mutations in bacterial genes, or by resistance genes being obtained through horizontal gene transfer between bacteria. Implant-infecting strains of *S. aureus* exhibit high rates of antibiotic resistance and include multidrug-resistant strains such as methicillin- and vancomycin-resistant *S. aureus*. There is also an alarming increase in antibiotic resistance observed in *S. epidermidis*, with up to 40% of *S. epidermidis* strains isolated from implant-associated and orthopaedic postsurgical infections being reported resistant to gentamicin [3].

2.2 Titanium as a biomaterial

There exists a variety of biomaterials that are used for medical implants, including metals and metal alloys, different polymeric materials and ceramics. Out of the metals and metal alloys used for medical implants, the front-runners include stainless steel, cobalt chromium alloys as well as titanium and titanium-based alloys. Titanium and titanium alloys have become the number one choice for orthopaedic implant materials and are used in everything from dental implants to fracture repair and hip replacement [8]. The reason behind the popularity of titanium and its alloys as a biomaterial for medical implants is the superior combination of properties such as mechanical strength, modulus of elasticity and biocompatibility. Titanium has a modulus of elasticity closer to that of cortical bone than other metals and its surface layer predictably oxidises upon implantation. The thin titanium oxide layer formed that coats the titanium implant is biologically inert and provide advantages such long-term material stability and lack of biological response [9]. In addition, titanium has the benefit that it osseointegrates in contact with bone, and thus ensures strong bonding and proper integration between the implant surface and the bone [8].

2.3 Gold nanorods

Gold nanorods have since the beginning of the 2000s been receiving increasing attention due to their tunable plasmonic properties and biocompatibility making them a promising candidate for a wide range of applications [10]. The applications where gold nanorods are being investigated span a broad range of research areas and include sensing, imaging, surface-enhanced spectroscopy and photothermal therapy. The unique properties of gold nanorods originate from the phenomena of localised surface plasmon resonance.

2.3.1 Localised surface plasmon resonance of gold nanorods

The physical and chemical properties of a material are, to a large extent, determined by the motion of its electrons. The electronic motions are in turn determined by the

type of material as well as the degree of spatial confinement imposed on the electrons. The spatial effects on electronic motion become prominent when the electrons in a material are confined to the nanoscale, i.e. on the length scale of 1-100 nm. In noble metals such as gold, reducing the particle size below the electron mean free path, which occurs in the 1-100 nm regime, gives rise to unique properties not present in the bulk materials. The unique properties of noble metal nanoparticles include strong absorption of light of specific frequencies, as reflected by the intense colours of their colloidal solutions [11].

When a gold nanoparticle is exposed to an electromagnetic wave, the oscillating electric field associated with the wave will cause a coherent oscillation of the free, conduction band, electrons of the particle. The coherent oscillation of electrons is known as a plasmon and the natural resonance frequency of the oscillation is called the plasmon resonance. The electron oscillation causes a charge separation between the metallic core and the free electrons of the particle, which in turn gives rise to a restoring Coulomb force, resulting in oscillation of the electron cloud with respect to the nuclei [12]. The coherent oscillation of electrons on a metallic nanoparticle is known as a localised surface plasmon (LSP). The spectral position of the localised surface plasmon resonance (LSPR) for gold nanoparticles is determined by the particle's size and shape, as well as the refractive index of the local environment [11]. The LSPR has two important effects on the properties of the gold nanoparticles. Firstly, the particles' optical extinction has a maximum at the LSPR frequency, causing a strong absorption of light and explaining the intense colours typical for gold nanoparticle colloids. Secondly, the electric fields near the particles' surfaces are greatly enhanced, with the enhancement rapidly decaying with the distance to the surface [13].

Spherical gold nanoparticles have one localised surface plasmon resonance frequency due to their symmetrical shape, and exhibit strong absorption in the visible region, commonly around 500 nm. For gold nanorods, the LSPR spectrum is split into two distinct bands; one transverse band corresponding to excitation of plasmons along the short axis of the particle, and one longitudinal band corresponding to excitation along the long axis. A general LSPR spectrum showing the transverse and longitudinal absorption bands of gold nanorods in dispersion is shown in Figure 2.1. The transverse band occurs in the visible region at similar wavelengths as for spherical gold nanoparticles and is insensitive to the size of the nanorods. The longitudinal band, which commonly occurs in the visible to near-infrared (NIR) region, exhibits stronger absorption, and the exact spectral position of the band depends on the aspect ratio (length/width) of the gold nanorods [11]. The optical absorption of gold nanorods can thus be tuned through the visible-NIR region by changing the dimensions of the particles, where an increase in aspect ratio causes a red-shift of the longitudinal band. The possibility to tune the optical properties of gold nanorods to absorb in the NIR region, commonly defined as the wavelengths 750-1500 nm, makes them suitable for biological applications, as this frequency region is known as the biological window where light penetration is optimal due to minimal absorption by water and haemoglobin in the tissue [11]. Gold nanorods that absorb light in the NIR region are therefore suited for *in vivo* applications as it enables the localised surface plasmon resonance to be externally induced.

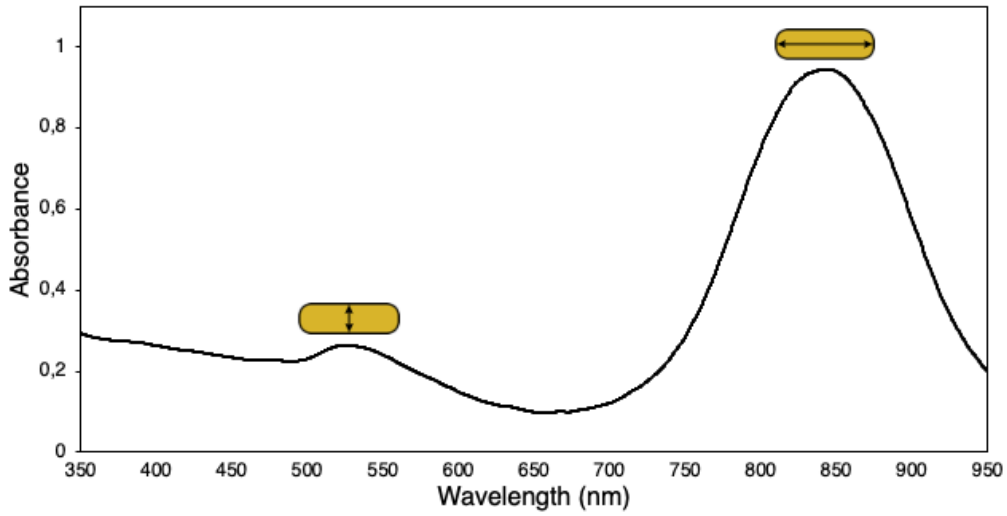

Figure 2.1: Localised surface plasmon resonance spectrum of gold nanorods showing the transverse and longitudinal absorption bands.

Exposing gold nanorods to light of their localised surface plasmon resonance frequency thus results in strong absorption of the light and subsequent plasmon formation. When the localised surface plasmons decay, the absorbed photon energy is distributed to conduction band electrons, generating electrons with a high effective temperature. The hot electrons relax by collisions with ions in the crystal lattice, resulting in heating of the gold nanoparticle crystal lattice via electron-phonon interaction. The lattice in turn cools by transferring its heat to the surrounding medium via phonon-phonon relaxation within a time scale of 100 ps [14]. The photothermal effect of gold nanorods upon exposure to light of their LSPR frequency makes them attractive for applications in the area of photothermal therapy.

2.3.2 Seed-mediated synthesis of gold nanorods

There exists various methods for the synthesis of gold nanorods, including both bottom-up approaches such as electrochemical methods and seed-mediated growth, as well as top-down approaches such as different lithography methods. Out of the different approaches, the wet chemical seed-mediated growth is the most common for the synthesis of colloidal gold nanorods due to the high quality and high yield of nanorods, the straightforward procedure and the simple particle dimension control [11]. The principle of the wet chemical seed-mediated synthesis procedure is that nucleation is firstly performed separately to produce a seed solution of small gold nanospheres, which subsequently is added to a growth solution wherein the nanorods are grown. One of the most common seed-mediated synthesis procedures that utilises the surfactant hexadecyltrimethylammonium bromide, also known as cetyltrimethylammonium bromide or simply CTAB, both to stabilise the seed and to act as a shape-directing agent during the nanorod growth was first reported in 2003 by Nikoobakht and El-Sayed [15]. CTAB remains the mostly employed surfactant in

the synthesis of gold nanorods due to the abundance of existing literature and to the surfactant fulfilling the basic requirements needed to achieve a rod-shape. CTAB, whose molecular structure is shown in Figure 2.2, has a carbon tail long enough to stabilise the nanorods, while still remaining short enough to attain solubility close to room temperature. Furthermore, CTAB contains a quarternary ammonium surfactant head group that forms a complex with the gold precursor and alters its redox potential, as well as bromide as a counter ion that has been shown to be crucial for the anisotropic growth process [10].

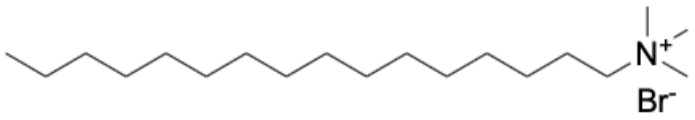

Figure 2.2: Chemical structure of hexadecyltrimethylammonium bromide (CTAB).

In the preparation of the seed solution, gold(III) chloride trihydrate ($HAuCl_4$) is reduced in the presence of CTAB with sodium borohydride, generating small (diameter typically below 4 nm) single-crystalline gold nanospheres [10]. The single-crystalline gold seeds are CTAB-capped and thereby stabilised from aggregating, with a positive surface charge due to the cationic ammonium head group. The growth solution consists of a mixture of $HAuCl_4$, CTAB and silver nitrate ($AgNO_3$), wherein the Au(III) from the $HAuCl_4$ is partially reduced to Au(I) by the addition of ascorbic acid. The presence of $AgNO_3$ facilitates rod formation and tunes the aspect ratio of the gold nanorods. The use of ascorbic acid as a reducing agent in the growth solution is crucial as ascorbic acid is not able to reduce gold ions to metallic gold under the high concentrations of CTAB and the low pH growth conditions, and instead partially reduces the Au(III) to Au(I). However, in the presence of the gold seed nanoparticles, complete reduction to Au(0) is catalysed by the surface of the seeds [11]. The final step in the gold nanorod synthesis is therefore addition of the gold seeds to the growth solution, which catalyses the final reduction step from Au(I) to Au(0) on the seeds' surfaces.

The seed-mediated synthesis method utilising CTAB-capped single-crystalline gold seeds and growth in the presence of silver nitrate produces single-crystalline gold nanorods with an octagonal cross section that grow longitudinally along the <100> direction [16]. The growth mechanism behind the formation of single-crystalline gold nanorods has received a large amount of attention and is still a matter of great interest. The initial view was that rod-shaped CTAB-micelles worked as a soft template for the gold nanorod growth, though this notion has evolved into the hypothesis that CTAB works as a face-specific capping agent that promotes anisotropic growth of the spherical gold seeds into rods [10]. Overall, there are strong implications that the specific binding of different species to distinct crystal facets of the gold nanorods during their growth is the major structure-directing aspect during the synthesis. Preferential binding of various species, mainly the CTA^+ cation, bromide and silver, to particular crystal facets on the gold nanorods influence the deposition rate of gold onto the facets, thereby determining the shape adapted during the growth.

2.3.3 Gold nanorod toxicity

When evaluating gold nanorods for biological applications, the aspect of their potential toxicity is important to consider. Gold in its bulk form is well studied and known to be a chemically inert material that is in general considered as safe [17]. As previously mentioned, when the size of a material is decreased into the 1-100 nm regime, new properties arise that are not present in their bulk form. The new properties that arise in nanomaterials are to a large extent why they are of interest for various applications, but also raise questions on what impact the properties have on the toxicity of the materials. For gold nanoparticles with dimensions larger than 5 nm, the general assumption is that the material is inert like its bulk form [17]. Though the cellular toxicity of gold nanorods, which in many cases are larger than 5 nm, is a quite complex issue as it is not only the gold nanorods themselves that need to be assessed.

A dispersion of gold nanorods synthesised with the seed-mediated synthesis described previously consists of at least three components; the gold nanorod core, the stabilising CTAB ligand capping the nanorods, and potential chemicals left over from the synthesis dissolved in the aqueous phase. Any toxicity observed for a dispersion of gold nanorods could thus be caused by either of these components. Studies have been conducted to evaluate the contribution of each component to the toxicity [17] [18] and has shown strong indications that rather than the actual gold nanorods, the CTAB desorbed from the nanorods along with CTAB and other reaction components left in the aqueous phase from the synthesis is what causes any observed toxicity.

2.4 Gold nanorod surface assembly

The assembly of gold nanorods into a variety of structures is an area that has gained much interest due to the possibility of affecting the nanorods' electronic and optical properties through their long-range ordering [16]. Assembling gold nanorods onto a surface could be of great importance for their practical application in numerous areas, and has for instance been examined for sensing [19]. The surface assembly of gold nanorods can be achieved through different approaches, where one of the more common ways is by utilising electrostatic interaction between the cationic nanorods and an anionic surface [16]. A disadvantage of using electrostatic interaction to assemble gold nanorods on surfaces is the sensitivity to ionic strength if immersed in a solution, which might cause the assembly to destabilise.

Another possible approach to the immobilisation of gold nanorods on surfaces is via chemisorption. For substrate surfaces of silicate glass or metal oxides, silanisation of the surface with a thiol-terminated alkoxysilane and subsequent gold nanorod attachment is one possible approach to chemisorption. An organosilane used for this purpose is (3-mercaptopropyl)trimethoxysilane (MPTMS). The surface assembly procedure includes immersion of the hydroxylated substrate in a solution of MPTMS in either ethanol or toluene, generating a thiol-terminated silane self-assembled monolayer on the surface [19]. The mercaptosilane-covered surface is thereafter incubated in an aqueous gold nanorod dispersion, which induces chemisorption of the nanorods

to the surface via thiol-gold bonding to the MPTMS molecules. A schematic representation of the surface assembly process is presented in Figure 2.3.

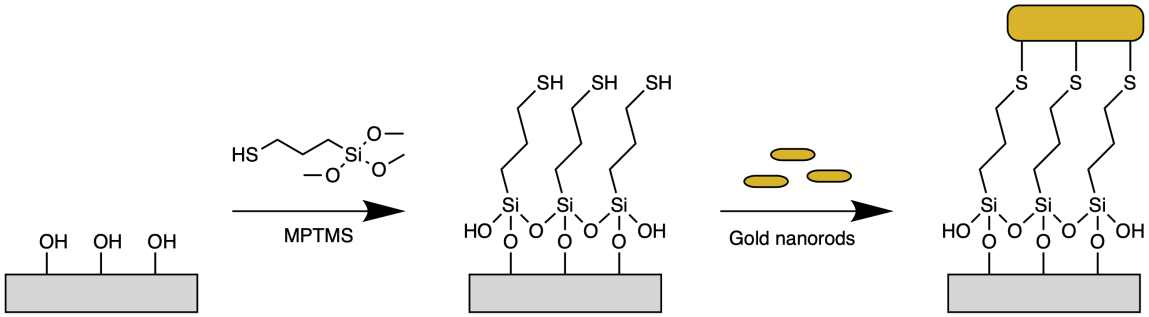

Figure 2.3: Schematic representation of the surface assembly of gold nanorods on silicate glass or metal oxide substrates using (3-mercaptopropyl)trimethoxysilane (MPTMS) as a linker.

3

Methods

The experimental work conducted during the thesis is presented in the following sections. The first section describes the materials used throughout the project, and is followed by a description of the seed-mediated synthesis procedures developed for the synthesis of gold nanorods. Thereafter, the surface assembly procedure used for producing the gold nanorod-functionalised surfaces in the project will be presented. A description of the *in vitro* studies with *Staphylococcus epidermidis* performed to evaluate the antimicrobial activity of the gold nanorod-functionalised surfaces upon irradiation with near-infrared light will also be presented. Lastly, the analytical techniques used throughout the thesis will be described, as well as in what characterisation purpose or purposes each technique was used.

3.1 Materials

For the synthesis of gold nanorods hexadecyltrimethylammonium bromide (≥98%, Sigma-Aldrich), gold(III) chloride trihydrate (≥99.9% trace metals basis, Sigma-Aldrich), sodium borohydride (99% ReagentPlus®, Sigma-Aldrich), hydrochloric acid (≥37%, Sigma-Aldrich), silver nitrate (99.9999% trace metals basis, Sigma-Aldrich) and L-ascorbic acid (99%, Sigma-Aldrich) were used as received. In the preparation of the gold nanorod-functionalised surfaces acetone (≥99.8%, VWR Chemicals), ethanol (95% analytical grade, Solveco), toluene (anhydrous max 0.002% water, VWR Chemicals), (3-mercaptopropyl)trimethoxysilane (95%, Sigma-Aldrich), ethanol (99.5% analytical grade, Solveco) and sodium chloride (≥99.5% ReagentPlus®, Sigma-Aldrich) were utilised. Milli-Q® water (18.2 MΩcm, Millipore) was used throughout the project.

All glassware used during the gold nanorod synthesis as well as during the preparation of the gold nanorod-functionalised surfaces was cleaned with basic piranha solution. The basic piranha solution was prepared with Milli-Q water, ammonia solution (28%, VWR) and hydrogen peroxide solution (30%, Fisher Scientific) in a 4:1:1 ratio. The solution was heated to 80°C and the cleaning allowed to proceed for approximately 15 min before the glassware was thoroughly rinsed with Milli-Q and dried with nitrogen gas.

3.2 Gold nanorod synthesis and purification

The gold nanorods used in the project were synthesised according to a seed-mediated synthesis procedure wherein nucleation is performed separately to make a seed solution of spherical gold nanoparticles, which is thereafter added to a growth solution to form the nanorods. Two sizes of gold nanorods were synthesised, and both procedures were adapted from methods described by Scarabelli and Liz-Marzán [10]. The gold nanorods with a higher aspect ratio (length/width) were synthesised to have a longitudinal absorption band in the near-infrared region around 850 nm, and the gold nanorods with a lower aspect ratio to have a longitudinal absorption band around 700 nm. Throughout the report the gold nanorods with a longitudinal band in the NIR region at 850 nm will be referred to simply as gold nanorods (AuNR). The nanorods with a longitudinal absorption at 700 nm will be referred to as gold nanorods 700 nm (AuNR700).

3.2.1 Seed-mediated synthesis of gold nanorods

The gold seed solution was prepared in a water bath at 30°C. Firstly, 25 μl of gold(III) chloride trihydrate ($HAuCl_4$) solution (50 mM) was added to 4.7 ml of CTAB solution (100 mM) and the mixture was mildly stirred until no signs of turbidity remained, approximately 10 min. In order to achieve the desired *in situ* formation of seeds through reduction of the gold salt precursor, 300 μl of sodium borohydride ($NaBH_4$) solution (10 mM) was thereafter added under strong stirring. After strongly stirring for 10 s, the light brown seed solution was mildly stirred and kept at 30°C until use.

The entire gold nanorod synthesis procedure was conducted in a water bath at 30°C. After adding 190 μl of hydrochloric acid (1 M) and 100 μl of $HAuCl_4$ solution (50 mM) to 10 ml of CTAB solution (100 mM), the mixture was gently stirred for 5 min. Thereafter, 120 μl of silver nitrate ($AgNO_3$) solution (10 mM) was added and the mixture was gently shaken for a few seconds. 100 μl of L-ascorbic acid solution (100 mM) was added to the growth solution and the solution thoroughly shaken, turning from yellow to colourless in a few seconds. Lastly, 24 μl of the prepared gold seed solution was added to the growth solution, the mixture was thoroughly shaken and then left undisturbed at 30°C for 2 h. The synthesis was successfully scaled up to five times the original amounts mentioned above.

3.2.1.1 Synthesis of gold nanorods 700 nm

In order to synthesise gold nanorods with a lower aspect ratio, and thus a longitudinal localised surface plasmon resonance at a shorter wavelength, a modified synthesis protocol was used. The gold nanorods with a lower aspect ratio were synthesised in order to evaluate, and possibly compensate for, any potential red-shift occurring for the LSPR frequency of the nanorods due to changes in refractive index arising once assembled on a titanium substrate. The magnitude of the red-shift was hypothesised to be between 100-200 nm, and the gold nanorods were therefore synthesised to have a longitudinal absorption band around 700 nm.

The same gold seed solution as described for the nanorods with a higher aspect ratio

in Section 3.2.1 was used in the synthesis. The entire synthesis of the gold nanorods 700 nm was conducted in a water bath at 28°C. Firstly, 100 μl of $HAuCl_4$ solution (50 mM) was added to 10 ml of CTAB solution (100 mM) and the mixture gently stirred for 10 min. Thereafter, 75 μl L-ascorbic acid solution (100 mM) was added and the solution was mixed thoroughly by shaking for a few seconds, turning colourless. 80 μl $AgNO_3$ (5 mM) was then added and mixed in by gently shaking for a few seconds. Lastly, 180 μl gold seed solution was added and the mixture vigorously shaken before being left undisturbed for 30 min at 28°C. The synthesis was successfully scaled up to three times the original amounts mentioned above.

3.2.2 Purification of gold nanorods

The purification of the synthesised gold nanorods was conducted through centrifugation. The as prepared gold nanorod synthesis solution was centrifuged at 1800 xg (28°C) for 40 min before the produced gold nanorod pellet was extracted with a pipette and re-dispersed in Milli-Q water. The centrifugation at 1800 xg for 40 min was subsequently repeated two additional times, yielding a total of three consecutive centrifugations. After the third centrifugation, the pellet of gold nanorods was re-dispersed in Milli-Q. The gold nanorod dispersions were stored at 4°C protected from sunlight.

3.2.3 Photothermal heating of gold nanorods in aqueous dispersion

The photothermal heating of the synthesised gold nanorods was evaluated by irradiating an aqueous dispersion of gold nanorods with a near-infrared laser while measuring the temperature change in the solution. The NIR laser used throughout the project was a LED M850L3 (900 mW, Thorlabs) with a spectral output at ∼800-870 nm and a maximum intensity at 850 nm. In a plastic cuvette, 3 ml of gold nanorod dispersion (1 nM) was irradiated with NIR light, and the temperature change over time was monitored using an alcohol thermometer inserted into the top part of the dispersion. As a control, the same procedure was performed with 3 ml of Milli-Q water.

3.3 Gold nanorod surface assembly

The substrates used for the preparation of gold nanorod-functionalised surfaces were titanium discs (9 mm diameter, 2 mm thickness) and glass pieces cut from microscopy slides (1.2 cm x 1.2 cm). The surface assembly procedure described below was used for both substrates.

The surfaces to be functionalised with gold nanorods were firstly cleaned in an ultrasonic cleaner in acetone for 20 min. Thereafter, the surfaces were rinsed thoroughly with Milli-Q water and dried with nitrogen gas (N_2), before an additional cleaning in an ultrasonic cleaner in ethanol (95%) for 20 min was conducted. The ethanol was carefully rinsed off with Milli-Q and the substrates dried with N_2. Fol-

lowing the ultrasonic cleaning, the surfaces were plasma treated with oxygen plasma for 7 min at 30 W (Extended Plasma Cleaner PDC-002 (230 V), Harrick Plasma). The plasma-treated surfaces were subsequently immersed in a solution of 2 vol% (3-mercaptopropyl)trimethoxysilane (MPTMS) in anhydrous toluene for 40 min, in order to assemble a monolayer of MPTMS on the surfaces. After 40 min, the surfaces were transferred to a glass beaker filled with ethanol (99.5%) and the ethanol was subsequently exchanged 3 times to ensure no MPTMS/toluene solution remained. Thereafter, the surfaces were transferred from the ethanol to a beaker containing Milli-Q water and the Milli-Q exchanged 4 times to remove any residual ethanol. Finally, the MPTMS-covered surfaces were immersed in a 0.5 nM gold nanorod dispersion in Milli-Q, to achieve surface assembly of the nanorods. Once the immersion in gold nanorod dispersion was completed, the gold nanorod-functionalised surfaces were rinsed thoroughly with Milli-Q and dried completely with N_2.

For assembling the gold nanorods 700 nm on titanium substrates, the same procedure as stated above was utilised with the only change implemented being the addition of sodium chloride (NaCl) to the gold nanorod dispersion. The dispersion of gold nanorods 700 nm used had a NaCl concentration of 5 mM.

3.3.1 Variation of surface coverage

The effect of the immersion time in the gold nanorod dispersion on the surface coverage of gold nanorods on the titanium discs was evaluated. The gold nanorod surface assembly procedure described above was utilised and the titanium discs where immersed in 0.5 nM gold nanorod dispersion in Milli-Q for 30, 60, 120, 180 and 240 min respectively.

3.3.2 Post-treatment of surfaces

The gold nanorod-functionalised titanium discs were post-treated with heat followed by oxygen plasma in order to (1) improve the surface attachment between the nanorods and the titanium substrate through sintering, and (2) reduce the potential toxicity of the gold nanorods by removing residual CTAB. The gold nanorod-functionalised titanium discs were first heat treated in a calcination oven at 300°C for 3 min. The discs were subsequently treated with oxygen plasma for 30 s at 30 W.

3.4 *In vitro* studies of photothermal elimination

To evaluate the antimicrobial activity of the gold nanorod-functionalised surfaces achieved upon irradiation with NIR light, *in vitro* studies were performed using *Staphylococcus epidermidis*. All surfaces used in the microbiology studies were firstly sterilised by immersion in ethanol (70%) for 20 min and subsequently moved through three water baths with sterile water to rinse.

S. epidermidis (ATCC 35984) was cultured on brain heart infusion agar at 37°C overnight and then kept at 4°C. One colony of *S. epidermidis* was cultured in tryptic soy broth overnight (17-18 h, 37°C) after which the bacteria were harvested by

centrifugation at 5000 xg for 5 min and resuspended in phosphate-buffered saline (PBS) supplemented with 0.5 g/l glucose. The bacterial suspension was thereafter centrifuged again (5000 xg, 5 min) and the bacteria subsequently resuspended in PBS with glucose (0.5 g/l) to a final concentration of 5×10^8 CFU/ml.

3.4.1 Gold nanorod-functionalised glass

To evaluate the antimicrobial activity of the gold nanorod-functionalised glass surfaces upon NIR irradiation, three different groups where used for the microbiology study. Triplicates were performed of each group. The three test groups were:

1. Glass irradiated with NIR light 5 min (Glass + NIR)
2. Gold nanorod-functionalised glass (GlassAuNR)
3. Gold nanorod-functionalised glass irradiated with NIR light 5 min (GlassAuNR + NIR)

The freshly prepared bacterial suspension (5×10^8 CFU/ml) was cultured on the glass surfaces for 2 h at 37°C, and the surfaces were then rinsed twice in PBS with glucose (0.5 g/l). The surfaces from group 1 and 3 where subsequently irradiated with overhead NIR light (LED M850L3, λ_{max}=850 nm, Thorlabs) for 5 min. Lastly, all samples were stained with LIVE/DEAD™ BacLight™ (ThermoFisher Scientific) and studied with a fluorescence microscope.

3.4.2 Gold nanorod-functionalised titanium

An equivalent *in vitro* study was performed for the gold nanorod-functionalised titanium discs to evaluate the antimicrobial activity upon NIR irradiation. An additional test group was included in order to evaluate the effect of the post-treatment of the surfaces on the heat-killing effect, yielding a total of four different groups. Triplicates were performed for each group. The four test groups were:

1. Titanium irradiated with NIR light 5 min (Ti + NIR)
2. Gold nanorod-functionalised titanium (TiAuNR)
3. Gold nanorod-functionalised titanium irradiated with NIR light 5 min (TiAuNR + NIR)
4. Gold nanorod-functionalised titanium (post-treated) irradiated with NIR light 5 min (TiAuNR + post-treat + NIR)

The freshly prepared bacterial suspension (5×10^8 CFU/ml) was cultured on the titanium surfaces for 2 h at 37°C, and the surfaces were then rinsed twice in PBS with glucose (0.5 g/l). The surfaces from group 1, 3 and 4 where subsequently irradiated with overhead NIR light for 5 min. Lastly, all samples were stained with LIVE/DEAD™ BacLight™ (ThermoFisher Scientific) and studied with a fluorescence microscope.

3.4.3 Gold nanorod 700 nm-functionalised titanium

An *in vitro* study with the gold nanorods 700 nm (AuNR700) surface assembled on titanium was also conducted. The microbiology study with the AuNR700 was performed in order to evaluate, and possible compensate for, a potential red-shift occurring for the LSPR frequency of the nanorods due to changes in refractive index arising ones surface assembled on titanium. Three test groups were used and each group was performed in triplicates. The test groups were:

1. Titanium irradiated with NIR light 5 min (Ti + NIR)
2. Gold nanorod 700 nm-functionalised titanium (TiAuNR700)
3. Gold nanorod 700 nm-functionalised titanium irradiated with NIR light 5 min (TiAuNR700 + NIR)

The freshly prepared bacterial suspension (5×10^8 CFU/ml) was cultured on the titanium surfaces for 2 h at 37°C, and the surfaces were then rinsed twice in PBS with glucose (0.5 g/l). The surfaces from group 1 and 3 where subsequently irradiated with overhead NIR light for 5 min. Lastly, all samples were stained with LIVE/DEAD™ BacLight™ (ThermoFisher Scientific) and studied with a fluorescence microscope.

3.5 Analytical techniques and characterisation

Throughout the project, various analytical techniques were utilised for characterisation. The following section will present each analytical technique as well as in what characterisation purpose, or purposes, it was implemented.

3.5.1 UV-Vis-NIR spectroscopy

UV-Vis-NIR spectroscopy refers to spectroscopy conducted using light in the ultraviolet, visible and near-infrared region of the electromagnetic spectrum. Spectroscopy in general is any analytical technique that measures interactions between matter and the electromagnetic spectrum. In UV-Vis-NIR spectroscopy, light is passed through a sample and the amount of light absorbed by the sample is determined from the difference between the incident light (I_0) and the transmitted light (I) [20]. The amount of light absorbed is commonly expressed as the absorbance (A), defined as:

$$A = -log(I/I_0)$$

Where the ratio between the transmitted and incident light, I/I_0, is the transmittance. The absorbance spectrum of a sample shows the absorbance as a function of wavelength [20]. In UV-Vis-NIR spectroscopy, typical wavelengths covered are 200-1500 nm.

UV-Vis-NIR spectroscopy was conducted throughout the project using a Thermo Scientific™ NanoDrop™ One^C Microvolume UV-Vis spectrophotometer, covering the wavelengths 200-850 nm. UV-Vis-NIR spectroscopy was performed on the synthesised gold nanorod dispersions in order to attain the localised surface plasmon resonance

spectra of the samples. The concentration of gold nanorods was derived from the absorbance spectra based on that an absorbance at 400 nm of 1.2 corresponds to [Au(0)]=0.5 mM, as described by Scarabelli and Liz-Marzán [10]. The relationship between particle concentration and absorbance originates from that gold nanoparticles with the same volume will equally contribute to the measured absorbance at 400 nm, as the main contribution to the absorbance at this wavelength comes from absorption related to interband transitions in metallic gold [10]. The gold nanorod concentrations obtained were compared with theoretical calculations and example calculations of both approaches are presented in Appendix A.1.

To evaluate the effect on the localised surface plasmon resonance spectrum of the gold nanorods once attached to a glass substrate, UV-Vis-NIR spectroscopy was performed on the gold nanorod-functionalised glass. The gold nanorod-functionalised glass was placed into a cuvette and UV-Vis-NIR spectra obtained with the sample both in air and immersed in Milli-Q water.

3.5.2 Scanning electron microscopy

A scanning electron microscope (SEM) is an electron microscope that produces an image of a sample by scanning it with a high-energy electron beam. The electron beam is thermoionically emitted from an electron gun fitted with a filament and it is focused down the electron column by a series of condensers and apertures. As the beam is scanned over the sample surface, the electrons in the beam interact with a limited volume of the sample. The electron-sample interactions produce various signals as the energies of the incident electrons are dissipated through repeated scattering and absorption events. The signals produced are detected by specialised detectors and include secondary electrons, back-scattered electrons as well as characteristic X-rays. For imaging of a sample, secondary and back-scattered electrons are commonly used. Secondary electrons originate from the atoms in the sample and are produced as a result of inelastic interactions between the electron beam and the sample [21]. As the secondary electron signal in the SEM is derived from secondary electrons originating from the surface region of the specimen, the images generated are surface sensitive and show the topography of the surface with high resolution. Back-scattered electrons originate from beam electrons that are elastically scattered by the specimen. Images generated from detecting back-scattered electrons give more information about differences in chemical composition as the fraction of incident electrons that escape as backscattered electrons increases with atomic number [21].

3.5.2.1 Visualisation of gold nanorod-functionalised surfaces

The gold nanorod-functionalised surfaces were visualised with a LEO Ultra 55 scanning electron microscope equipped with a field emission gun. The surface coverage of gold nanorods on the prepared surfaces, as well as the nanorods' dimensions, were determined through image analysis of the obtained SEM micrographs using the image processing program Fiji (ImageJ, National Institute of Health, USA). Furthermore, SEM was used to evaluate how the post-treatment of the gold nanorod-functionalised titanium affected the dimensions and the shape of the gold nanorods.

3.5.2.2 Bacterial morphology studies

Scanning electron microscopy was used to visualise the samples from the *in vitro* studies in more detail, in order to further evaluate the effects of the gold nanorods and the NIR light on the bacteria. The bacteria-covered samples were prepared for the SEM by fixation in 4% formaldehyde overnight at 4°C. Thereafter, the samples were stepwise dehydrated in ethanol (20, 40, 60, 80 and 99.5%) for 10 min per step. A final drying was performed by immersing the samples in a 1:1 mixture of hexamethyldisilazane (HDMS) and ethanol (99.5%) for 15 min, followed by immersion in 100% HDMS for 15 min. Lastly, the HDMS was removed and the samples left in a fume hood until all residual HDMS had evaporated. The glass samples were also gold-sputtered before visualisation in the SEM.

3.5.3 X-ray photoelectron spectroscopy

X-ray photoelectron spectroscopy (XPS) is a surface sensitive and non-destructive analysis technique used to determine the elemental composition of the surface of a sample. In XPS, the sample is irradiated with X-ray photons, which collide with and thereby remove electrons from the atoms in the sample. An emitted photoelectron's kinetic energy, which is equal to the difference in energy between the incident photon and the binding energy of the electron to the nucleus, is measured. Characteristic energies of the emitted photoelectrons from different electron shells of elements are detected and a photoelectron spectrum is acquired by counting emitted electrons over a range of kinetic energies. From the XPS spectrum, the chemical composition and state of the individual elements in the sample's surface layer can be characterised [22].

X-ray photoelectron spectroscopy was performed on the gold nanorod-functionalised titanium discs using a PHI 5000 VersaProbe III Scanning XPS Microprobe, in order to determine the elemental composition and chemical state of the specimens' surfaces. The efficiency of the post-treatment in removing the remaining CTAB from the surface assembled gold nanorods was evaluated by comparing one untreated and one post-treated sample.

3.5.4 Fluorescence microscopy

Fluorescence microscopy is a type of optical microscopy that utilises fluorescence to generate an image. A fluorescence microscope uses a light source, commonly mercury-vapour or xenon arc lamps, that produces light of specific wavelengths in the UV-Vis region. When the specimen is illuminated, the fluorophores in the specimen absorb light of a specific wavelength region and then, within nanoseconds, emit light in a different, longer, wavelength region. By completely filtering out the exciting light without blocking the emitted fluorescence, it is possible to visualise only the fluorescent objects in the specimen [23]. In order for a sample to be suitable for fluorescence microscopy it must thus either contain fluorophores, which commonly is achieved by labelling with fluorescent probes, or exhibit autofluorescence.

Fluorescence microscopy was performed during the *in vitro* studies using an Axio

Imager Z2m microscope (Zeiss) equipped with an HBO-lamp for fluorescence imaging. After NIR irradiation, the samples were stained with LIVE/DEAD™ BacLight™ (ThermoFisher Scientific) that monitor bacterial cell viability depending on cell membrane integrity. The staining contains a green-fluorescent nuclei acid stain that penetrates all cells, and a red-fluorescent nucleic acid stain that only penetrates cells with impaired membranes [24]. The stained samples were visualised at 40x magnification and the amount of eliminated bacteria was evaluated through image analysis (Fiji), in terms of the area covered by dead (red) and live (green) bacteria.

4

Results and discussion

In the following sections the principal results achieved during the thesis will be presented and discussed. Firstly, the results from the characterisation of the gold nanorods in terms of localised surface plasmon resonance spectra and dimensions will be presented. Following will be a description of the gold nanorod-functionalised surfaces produced during the project. Lastly, the results from the *in vitro* studies performed will be demonstrated and interpreted, followed by a short discussion of the gold nanorods' potential toxicity.

4.1 Characterisation of gold nanorods

The section will present the results from the characterisation of both sizes of the gold nanorods synthesised with the seed-mediated synthesis procedures. The localised surface plasmon resonance spectra of the gold nanorods in aqueous dispersion will first be shown, followed by the dimensions of the gold nanorods. Lastly, the photothermal heating of the gold nanorods dispersed in Milli-Q, upon irradiation with NIR light, will be presented.

4.1.1 Localised surface plasmon resonance spectra of gold nanorods

The UV-Vis-NIR spectroscopy performed on the synthesised gold nanorods dispersed in Milli-Q showed that the gold nanorods (AuNR) exhibited a localised surface plasmon resonance spectrum with a transverse absorption band at 510-530 nm and a longitudinal band at 800-850 nm. The longitudinal absorption band at 800-850 nm thus matched the spectral output of the NIR laser intended to be used throughout the project. The gold nanorods 700 nm (AuNR700) also had a transverse absorption band around 510-530 nm, while the longitudinal band was at 680-710 nm. Examples of localised surface plasmon resonance spectra for both the sizes of synthesised gold nanorods are presented i Figure 4.1.

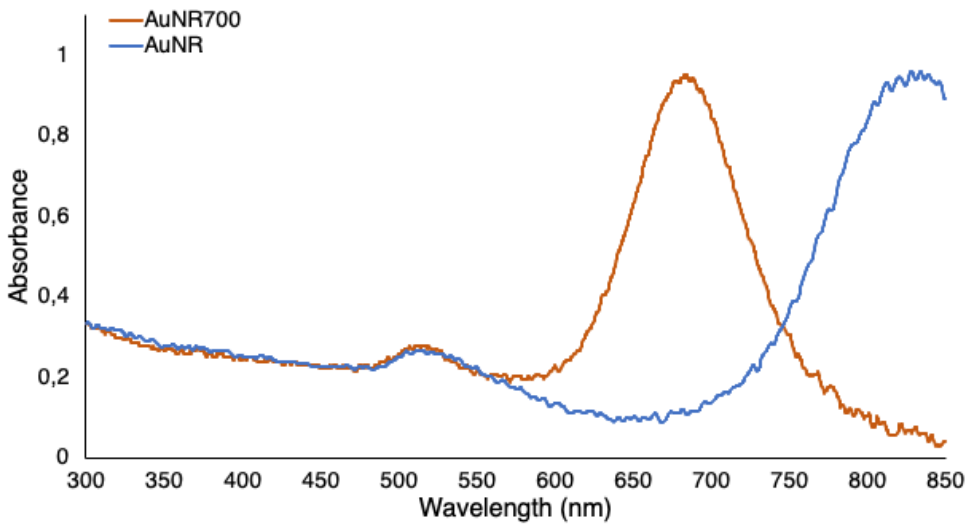

Figure 4.1: Localised surface plasmon resonance spectra of the synthesised gold nanorods, of both aspect ratios, dispersed in Milli-Q.

4.1.2 Gold nanorod dimensions

The average dimensions of both aspect ratios of gold nanorods, as determined through image analysis of SEM micrographs, are presented in Table 4.1. The gold nanorods (AuNR) had an average length of 64 nm, an average width of 20 nm and an average aspect ratio (length/width) of 3.4. The average dimensions were determined by analysing a total of 5735 gold nanorods. The gold nanorods 700 nm (AuNR700) had an average length of 43 nm, an average width of 17 nm and an average aspect ratio of 2.6. The average dimensions were determined by analysing a total of 1029 gold nanorods 700 nm.

	AuNR	**AuNR700**
Length (nm)	64.0 ± 9.8	42.6 ± 5.2
Width (nm)	19.8 ± 4.3	17.0 ± 2.9
Aspect ratio (length/width)	3.39 ± 0.77	2.57 ± 0.47

Table 4.1: Average dimensions of gold nanorods determined through image analysis of SEM micrographs.

4.1.3 Photothermal heating of gold nanorods in aqueous dispersion

During 15 min NIR irradiation of the aqueous dispersion of gold nanorods (1 nM), a total temperature increase from 19.8°C to 31.5°C was observed. After 15 min NIR irradiation of the control with Milli-Q, a temperature increase from 20°C to 20.5°C was measured. The gold nanorods thus increased the temperature of the surrounding aqueous phase a total of 11.2°C compared to the control. The temperature increase

measured for the gold nanorod dispersion clearly shows the photothermal heating caused by the NIR light generating localised surface plasmons, that subsequently decay and transfer their energy to the surrounding as heat.

4.2 Characterisation of gold nanorod-functionalised surfaces

The scanning electron microscopy performed on the gold nanorod-functionalised titanium and glass surfaces revealed an even coverage of gold nanorods over the surfaces. The gold nanorods were randomly oriented on the surfaces and had not formed any larger aggregates. Figure 4.2 shows representative SEM micrographs (50 000x magnification) of gold nanorod-functionalised titanium and glass, respectively. The surfaces in Figure 4.2 were prepared with a 0.5 nM dispersion of gold nanorods and an immersion time of 4 h. A side view of the surface assembled gold nanorods on titanium is presented in Figure A.1, Appendix A.2, showing the random orientation of the nanorods on the surface. A representative SEM image (100 000x magnification) of the gold nanorods 700 nm assembled on titanium is presented in Figure A.2, also in Appendix A.2.

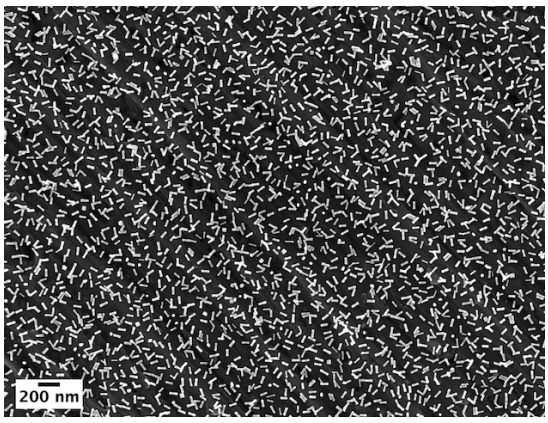

(a) Gold nanorod-functionalised titanium

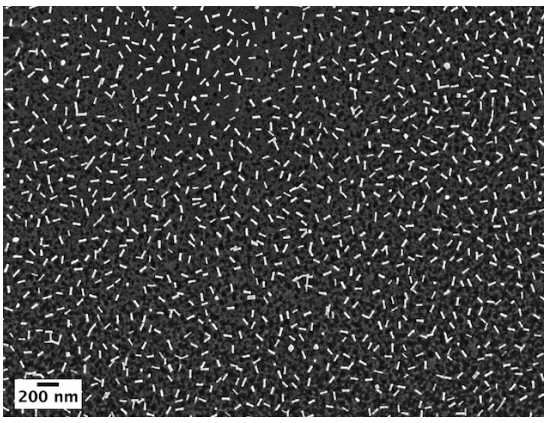

(b) Gold nanorod-functionalised glass

Figure 4.2: SEM micrographs at 50 000x magnification of gold nanorods surface assembled on titanium and glass substrates.

As shown by the SEM micrographs in Figure 4.2, there is a distinct difference in the surface coverage of gold nanorods on the titanium substrate compared to the glass substrate, despite both samples being prepared in an equivalent way. After 4 h immersion in 0.5 nM gold nanorods dispersed in Milli-Q, the titanium surface had a coverage of approximately 20%, corresponding to 158 nanorods/μm^2, while the glass was only covered to about 9%, corresponding to 71 nanorods/μm^2. Why the surface coverage of gold nanorods achieved is different between the titanium and glass substrates is likely due to differences in surface chemistry. The glass substrates used were cut from microscopy slides, which do not consist of 100% silicon dioxide

but is doped with other compounds. This means that it is likely that the amount of hydroxyl groups present on the surface after the oxygen plasma treatment is lower for the glass than the titanium. In turn this would cause a lower amount of MPTMS to be present on the glass surfaces, and consequently a lower amount of gold nanorods to be attached. There are also differences in surface roughness between the two materials, where the glass has a much lower roughness compared to the titanium, which might also effect the coverage of gold nanorods achieved.

4.2.1 Variation of surface coverage

The variation of the surface coverage of gold nanorods on the titanium discs, determined through image analysis of SEM micrographs, with different immersion times in gold nanorods dispersed in Milli-Q (0.5 nM) is presented in Figure 4.3. The surface coverage increased from 5-6% for 30 min immersion time (39-47 gold nanorods/μm^2) to 19-21% after 240 min immersion (150-165 gold nanorods/μm^2). From the trend seen in the increase of surface coverage with immersion time in Figure 4.3, the coverage of gold nanorods on the titanium surface could likely only have been increased slightly more by even longer immersion time than 240 min. Between 180 min and 240 min the surface coverage increased from 18-20% to 19-21%, indicating that the surfaces were more or less "saturated" with nanorods by then. This saturation is likely due to electrostatic repulsion between the cationic nanorods. If an even higher surface coverage was desired, the ionic strength of the gold nanorod dispersion could be tuned in order the screen the charges of the nanorods.

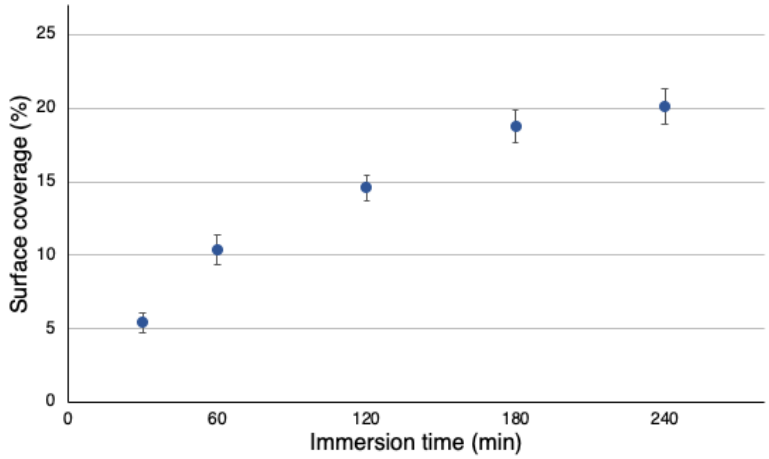

Figure 4.3: Surface coverage of gold nanorods on titanium as a function of immersion time in 0.5 nM gold nanorod dispersion in Milli-Q.

No further evaluation of the surface coverage of gold nanorods on titanium was conducted as it was deemed too time consuming, and as a much higher surface coverage than the 20% achieved with the gold nanorods dispersed in Milli-Q was not desired. The reason for not desiring a too high surface coverage of gold nanorods was in relation to the aimed application for the gold nanorod-functionalised titanium. To be

applied on medical implants, it is preferred for the majority of the implant surface exposed to the surrounding tissue to be Ti/TiO_2 in order to achieve good integration. It is thus not reasonable to have a surface coverage of 50% gold nanorods as that with high likelihood would impede on the properties of the titanium implant.

4.2.2 X-ray photoelectron spectroscopy

The gold nanorod-functionalised titanium discs that were characterised with X-ray photoelectron spectroscopy had a surface coverage of 11-12% (87-94 nanorods/μm^2). The chemical compositions of the untreated and the post-treated gold nanorod-functionalised titanium is presented in terms of atomic concentration in Table 4.2. The full survey spectra showing the counts versus binding energy for both samples can be found in Appendix A.3. The Ti 2p doublet peak at approximately 460 eV present in the survey spectra of both samples is attributed to Ti 2p in Ti^{4+}, which shows that the main component of the titanium surface layer is TiO_2. That the top layer of the titanium discs consist of TiO_2 is expected as the discs are treated with oxygen plasma during the surface assembly procedure. The titanium oxide layer further explains the large amount of oxygen present in both samples, where the slightly higher value for the post-treated surface, 55% compared to 51%, can be explained by the additional oxygen plasma treatment performed after the gold nanorod-surface assembly. Most samples that have been exposed to air will have a detectable amount of adventitious carbon on them, which together with the presence of carbon in the CTAB capping the gold nanorods as well as in the MPTMS used to link the gold nanorods to the substrate, can explain the 15-20 % carbon detected in the samples.

Sample	Atomic concentration (%)							
	C 1s	**N 1s**	**O 1s**	**S 2p**	**Ti 2p**	**Br 3d**	**Ag 3d**	**Au 4f**
TiAuNR	20.02	1.52	51.37	0.45	17.77	0.50	1.43	6.95
TiAuNR post-treated	16.11	1.21	55.31	0.66	18.25	-	1.25	6.39

Table 4.2: Atomic concentration table from X-ray photoelectron spectroscopy measurements on untreated (TiAuNR) and post-treated (TiAuNR post-treated) gold nanorod-functionalised titanium.

The atomic concentrations from the XPS characterisation in Table 4.2 clearly shows the presence of gold from the gold nanorods on the surfaces, constituting approximately 6-7%. Furthermore, relatively high levels of nitrogen and silver, between 1-2%, were detected in both samples. Nitrogen is expected as a component of both CTAB and MPTMS. The silver likely remains on the gold nanorods from the synthesis, where silver is added in the form of $AgNO_3$ as a shape-directing agent. Lastly, the 0.4-0.7% of sulphur can be linked to MPTMS and the 0.5 % of bromine detected on the untreated sample to the bromide counterion of CTAB.

4.2.3 Evaluation of surface post-treatment

The effects of the heat and oxygen plasma post-treatment on the gold nanorod-functionalised titanium surfaces were evaluated by both visualisation of the surface as-

sembled gold nanorods using SEM, and by evaluating changes in the chemical composition with XPS. A comparison of the average dimensions of the gold nanorods assembled on titanium with and without the post-treatment showed that a slight decrease in dimensions could be observed for the post-treated gold nanorod-functionalised titanium. On average, the gold nanorods' length decreased with 2.4 nm, the width with 0.48 nm and the aspect ratio with 0.04. The average decrease in dimensions was determined by analysing 823 gold nanorods before post-treatment and then 1235 nanorods after the post-treatment. The observed decrease of the nanorods' dimensions shows that the post-treatment affects the gold nanorods, but to such a small extent that the localised surface plasmons resonance frequency should not be effected to any large degree as the aspect ratio remains virtually unaffected. A slight change in the shape of the gold nanorods could also be noted between the untreated and post-treated specimens as shown by the SEM micrographs (150 000x magnification) in Figure 4.4. The untreated gold nanorods in Figure 4.4a had a more angular shape, whereas the post-treated nanorods in Figure 4.4b had adapted a more rounded shape. Furthermore, in the post-treated sample the gold nanorods that were in contact with each other appeared to have merged together. Altogether, the observed effects give clear indication that the post-treatment induced a sintering of the gold nanorods.

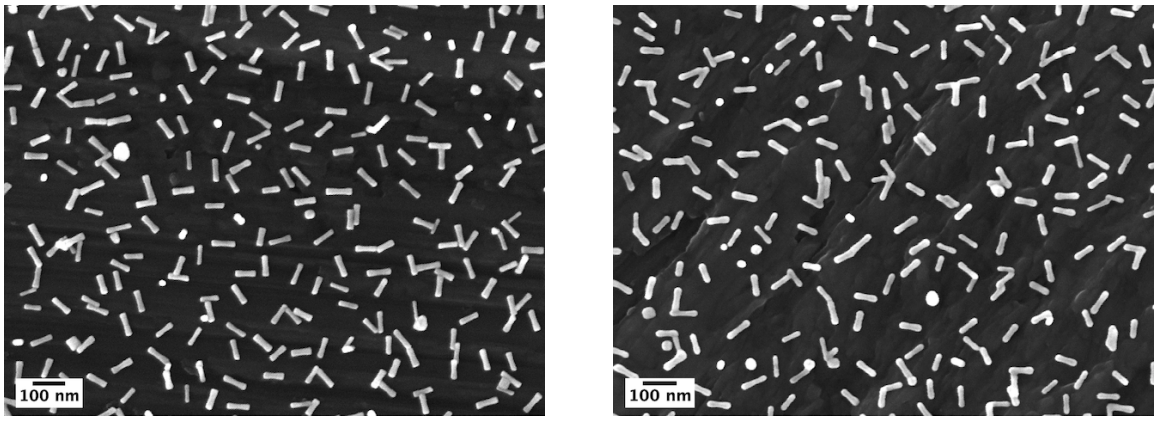

(a) Untreated **(b)** Post-treated

Figure 4.4: SEM micrographs at 150 000x magnification of untreated and post-treated gold nanorod-functionalised titanium.

The differences in chemical composition between the untreated and the post-treated gold nanorod-functionalised titanium surfaces, shown by the atomic concentrations determined with XPS in Table 4.2, provide clear evidence that the post-treatment is effective in removing the CTAB from the surface assembled gold nanorods. The CTAB capping the gold nanorods is the only component in both the gold nanorod synthesis and the surface assembly procedure that contains bromine. The fact that no bromine could be detected on the post-treated surface is thus a strong indication that the post-treatment is efficient. The lower amounts of carbon and nitrogen detected on the post-treated surface compared to the untreated one further supports the notion that the CTAB is successfully removed. As mentioned in Section 2.3.3, it has been shown that CTAB that has desorbed from gold nanorods may exhibit a

certain toxicity. The successful removal of CTAB from the surface assembled gold nanorods thereby show promise for potential biological applications as it reduces the risk of the gold nanorod-functionalised surfaces exhibiting any toxicity.

4.2.4 Localised surface plasmon resonance spectrum of gold nanorod-functionalised glass

The effect on the localised surface plasmon resonance spectrum of the synthesised gold nanorods assembled on a glass substrate, as determined by UV-Vis-NIR spectroscopy of the gold nanorod-functionalised glass, is shown in Figure 4.5. Compared to the LSPR spectrum of gold nanorods dispersed in Milli-Q, see Figure 4.1, the absorption bands are in general lower, as expected by the lower concentration of gold nanorods on the glass substrate compared to in dispersion. The longitudinal absorption band is also wider for the gold nanorods assembled on glass. The widening of the absorption band could be due to plasmon coupling between the gold nanorods, i.e. an interaction of the localised surface plasmon resonances when the nanorods come in close proximity of each other. Plasmon coupling occurs when the gold nanorods are within a distance of 2.5 times the nanorods' diameter [25], and once assembled on a substrate the distances between the nanorods are on the scale of tens of nanometers with some nanorods being physically in contact with each other.

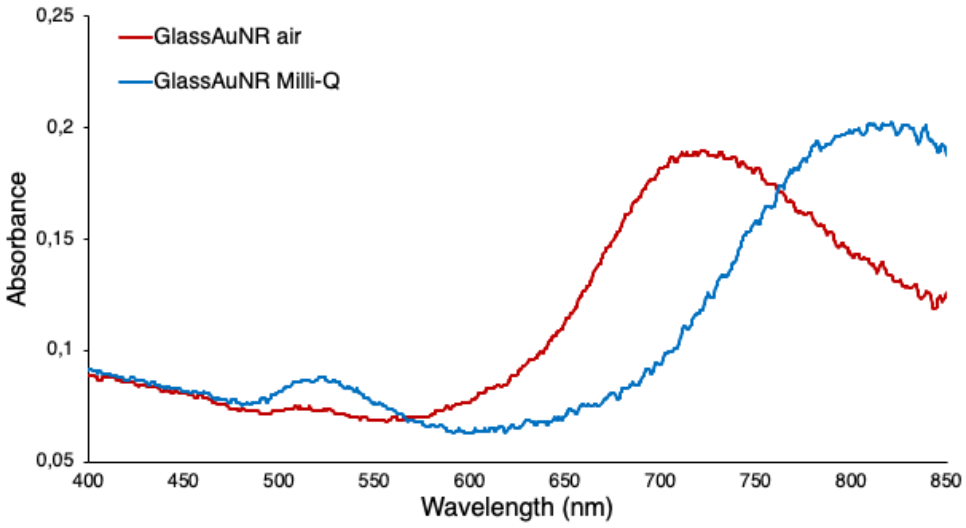

Figure 4.5: Localised surface plasmon resonance spectra of gold nanorod-functionalised glass in air and immersed in Milli-Q.

The localised surface plasmon resonance spectra of the gold nanorods assembled on glass in Figure 4.5 clearly show how the spectral position of the longitudinal absorption band changes with the refractive index of the surrounding environment. By comparing the UV-Vis-NIR spectroscopy measurement performed in air, which has a refractive index of 1, and in Milli-Q, which has a refractive index of 1.33, a red-shift occurs for the longitudinal peak of approximately 125 nm.

4.3 *In vitro* studies of photothermal elimination

In the following section the results from the *in vitro* studies conducted with *S. epidermidis* cultured on gold nanorod-functionalised glass respectively titanium will be presented. The results from the study on glass will be presented and discussed first, followed by the studies performed on titanium. Lastly, a section discussing the potential toxicity of the surface assembled gold nanorods will be included.

4.3.1 Gold nanorod-functionalised glass

The gold nanorod-functionalised glass surfaces used in the *in vitro* study to evaluate the antimicrobial activity of the surfaces upon NIR irradiation had an average surface coverage of 7-10%. The surface coverage corresponds to 55-79 gold nanorods/μm^2. From the fluorescence microscopy performed on the surfaces stained with LIVE/DEAD™ staining, a difference in the amount of dead (red) and live (green) bacteria could be observed between the control groups and the gold nanorod-functionalised glass that had been exposed to NIR light. Representative images from the fluorescence microscopy are presented in Figure 4.6. Figure 4.6a shows the bare glass irradiated with NIR for 5 min (Glass + NIR), Figure 4.6b shows the non-irradiated gold nanorod-functionalised glass (GlassAuNR), and Figure 4.6c the gold nanorod-functionalised glass irradiated with NIR for 5 min (GlassAuNR + NIR). The gold nanorod-functionalised glass irradiated with NIR light has a larger amount of dead bacteria compared to both control surfaces, indicating that there in fact occurs a photothermal elimination of the *S. epidermidis* due to the localised surface plasmon resonance-generated heat from the gold nanorods.

The results from the image analysis of the fluorescence images for all three replicates determining the area covered by dead (red) cells and live (green) cells is presented in Figure 4.7. The average percentage of dead bacteria for the Glass + NIR was 54% and for the GlassAuNR 52%, while the average percentage for the GlassAuNR + NIR was 78%. There was thus between 40-50% more dead bacterial cells on the gold nanorod-functionalised glass irradiated with NIR compared to the control groups, clearly showing an antimicrobial activity being achieved upon NIR irradiation of the glass functionalised with gold nanorods. When performing a Wilcoxon rank sum test on the data from the image analysis, a significant difference could be shown between the percentage of dead bacteria on the GlassAuNR + NIR and each of the two control groups, with a significance level of 1%.

The relatively high percentage of dead bacteria present in both control groups could likely be due to the usage of an overnight culture of *S. epidermidis*, meaning that the bacteria was not in the optimal growth phase once cultured on the glass surfaces. A more prominent difference between the controls and the gold nanorod-functionalised glass exposed to NIR could probably have been achieved if the bacteria was cultured on the surfaces during a better growth phase. Furthermore, by utilising surfaces with a higher surface coverage of gold nanorods, meaning that each bacterium would be exposed to a larger number of nanorods, the antimicrobial activity could have been improved.

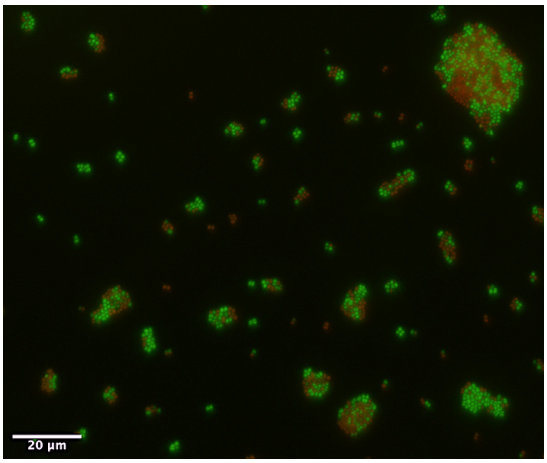

(a) Glass + NIR

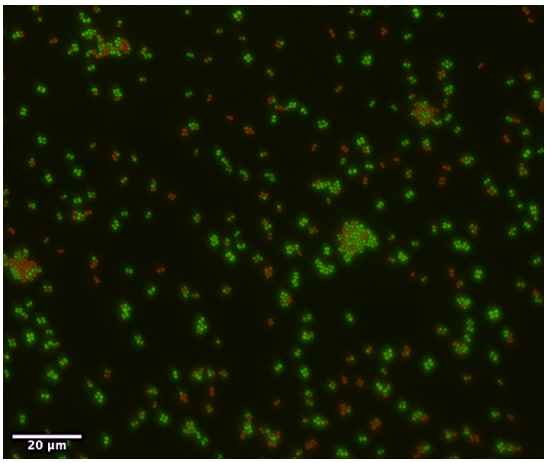

(b) GlassAuNR

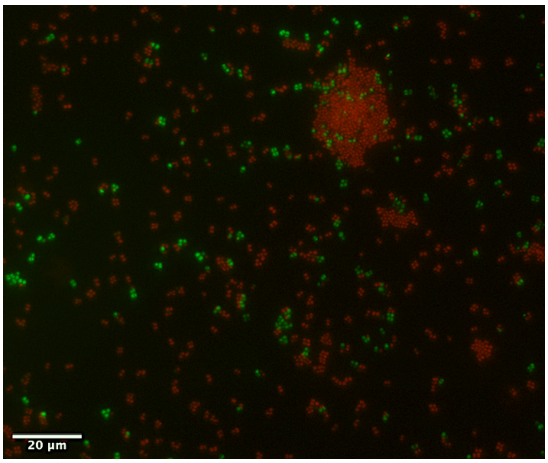

(c) GlassAuNR + NIR

Figure 4.6: Images from fluorescence microscopy of samples after LIVE/DEAD™ staining from the *in vitro* study with *S. epidermidis* on gold nanorod-functionalised glass.

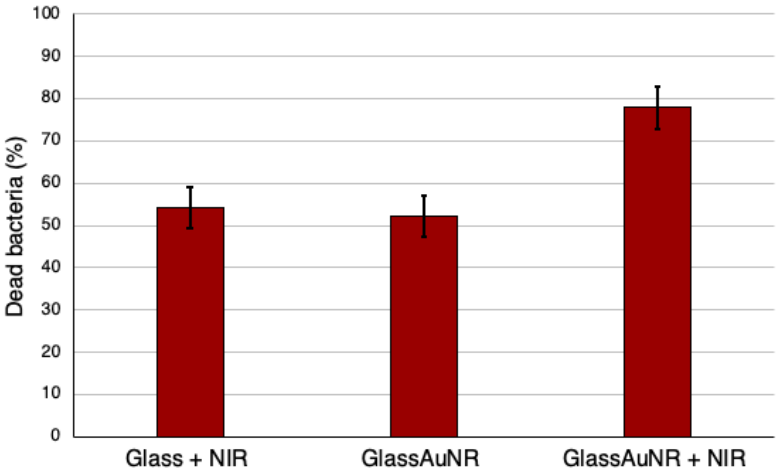

Figure 4.7: Percentage of dead bacteria covering the surfaces from the *in vitro* study with *S. epidermidis* on gold nanorod-functionalised glass.

4.3.1.1 Bacterial morphology study

By studying the surfaces from the *in vitro* study on glass in the SEM, a difference in bacterial morphology could be discerned between the bacteria on the control surfaces and the bacteria on the gold nanorod-functionalised glass irradiated with NIR light. As shown in Figure 4.8a and 4.8b, the bacteria on the control surfaces had a spherical and smooth shape, while some of the bacteria on the gold nanorod-functionalised glass exposed to NIR light, shown in Figure 4.8c, looked more shrivelled and punctured. The differences in morphology can be seen as an indication of the heat-killing effect caused by NIR irradiation of the gold nanorods, but it is important to remember than only a small fraction of the bacteria was visualised in the SEM and thus further investigations are needed in order to draw more solid conclusions.

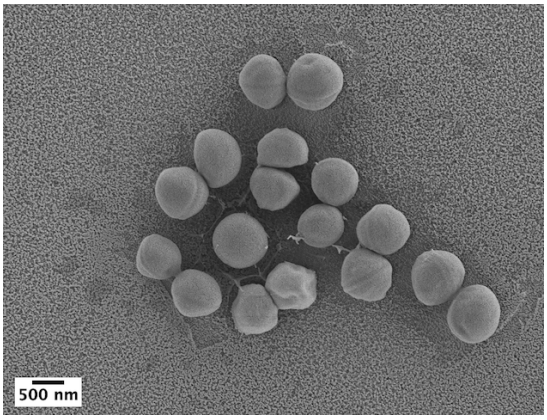

(a) Glass + NIR

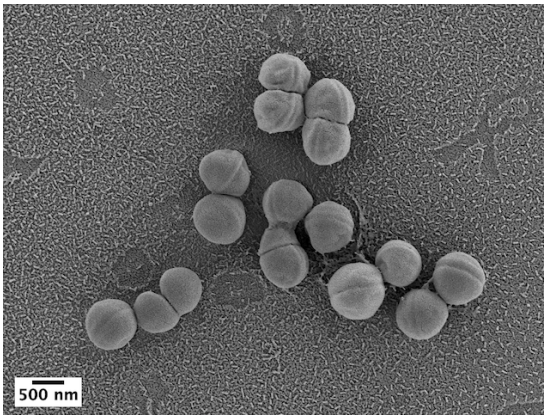

(b) GlassAuNR

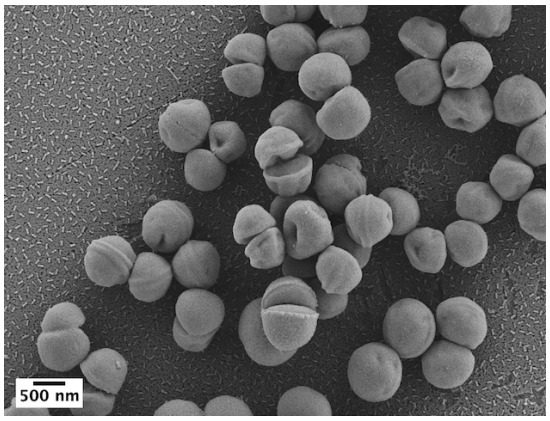

(c) GlassAuNR + NIR

Figure 4.8: SEM micrographs at 30 000x magnification of *S. epidermidis* on surfaces from the *in vitro* study on gold nanorod-functionalised glass.

4.3.2 Gold nanorod-functionalised titanium

The gold nanorod-functionalised titanium surfaces used in the *in vitro* study to evaluate the antimicrobial activity of the surfaces upon NIR irradiation had an average surface coverage of 16-17%. The surface coverage corresponds to 126-134 gold

nanorods/μm^2. From the fluorescence microscopy performed on the surfaces stained with LIVE/DEAD™ staining, no significant difference in the amount of dead (red) and live (green) bacteria could be noticed between the four test groups. Representative images from the fluorescence microscopy are shown in Figure 4.9.

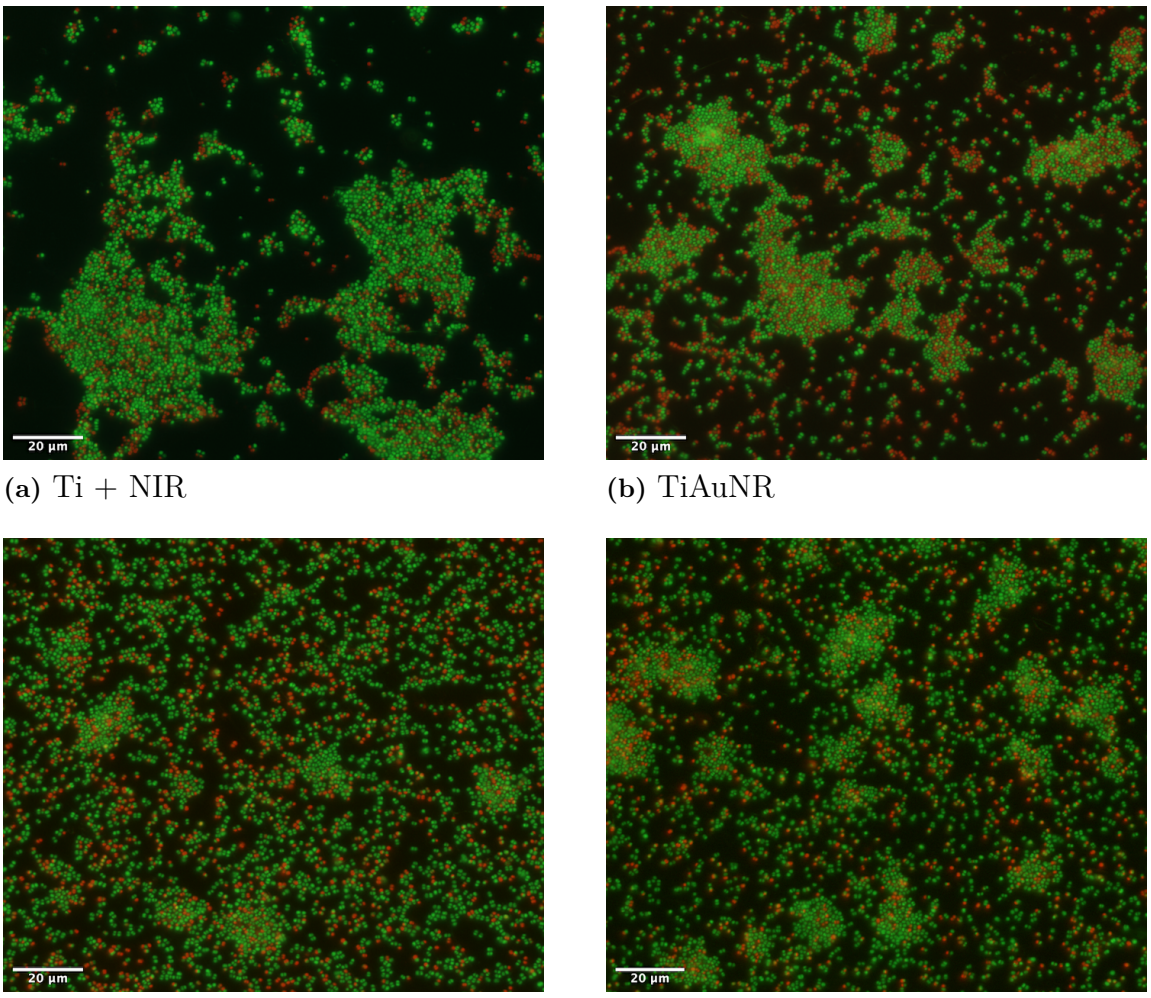

(a) Ti + NIR

(b) TiAuNR

(c) TiAuNR + NIR

(d) TiAuNR + post-treat + NIR

Figure 4.9: Images from fluorescence microscopy of samples after LIVE/DEAD™ staining from the *in vitro* study with *S. epidermidis* on gold nanorod-functionalised titanium.

The results from the image analysis of the fluorescence images determining the area covered by dead (red) and live (green) bacteria, for all three replicates, is presented in Figure 4.10. The average percentage of dead bacteria for the bare titanium irradiated with NIR light for 5 min (Ti + NIR) was 28%, for the non-irradiated gold nanorod-functionalised titanium (TiAuNR) 36%, for the gold nanorod-functionalised titanium exposed to NIR (TiAuNR + NIR) 37%, and the post-treated gold nanorod-functionalised titanium exposed to NIR (TiAuNR + post-treat + NIR) 30%. Even though the average percentages of dead bacterial cells were somewhat different between the test groups, the amount of dead bacteria present on the surfaces varied between the replicates, preventing any certain differences from being determined.

When performing a Wilcoxon rank sum test with a significance level of 1% on the data from the image analysis, no significant difference could be shown between the percentage of dead bacteria on the TiAuNR + NIR compared to each of Ti + NIR and TiAuNR. No significant difference could be shown between the percentage of dead bacteria on the TiAuNR + post-treat + NIR compared to each of the Ti + NIR and TiAuNR either. No evident antimicrobial activity of the gold nanorod-functionalised titanium exposed to NIR light could thus be shown from the *in vitro* study.

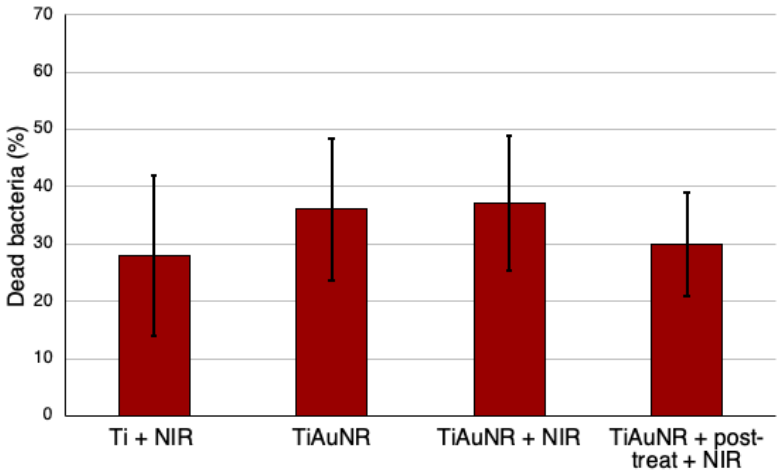

Figure 4.10: Percentage of dead bacteria covering the surfaces from the *in vitro* study with *S. epidermidis* on gold nanorod-functionalised titanium.

There are multiple possible reasons as to why no antimicrobial activity could be observed for the titanium surfaces in comparison to the glass surfaces. Firstly, as mentioned in the Section 2.3.1, the spectral position of the localised surface plasmon resonance of gold nanorods is in part determined by the refractive index of their surroundings. In the gold nanorod dispersions used for the UV-Vis-NIR spectroscopy to determine the LSPR spectra of the nanorods, the nanorods are surrounded by water that has a refractive index of 1.33. Glass has a refractive index between 1.5-1.6 [26], depending on the exact chemical composition. When the gold nanorods are assembled on glass, the refractive index of the surroundings therefore changes only slightly compared to when the nanorods are dispersed in water, and as shown by the LSPR spectra of the gold nanorod-functionalised glass in Figure 4.5 the nanorods still absorb light around 850 nm. The refractive index of titanium is around 2.1, while the refractive index of titanium dioxide varies between 2.5-2.9 depending on the crystal structure [26]. When assembling the gold nanorods on the oxide-covered titanium substrates, the refractive index of the surrounding environment might thus almost double compared to the nanorods dispersed in water. As the LSPR frequency of gold nanorods red-shift as the refractive index of the surroundings increases, it is possible that the spectral output of the NIR laser used, with a maximum output at 850 nm, does not match the resonance frequency of the nanorods once they are assembled on titanium. If this is the case, no formation of localised surface plasmons would occur and consequently no heat would be generated by the gold nanorods.

Another possible explanation as to why no antimicrobial activity could be noticed for the gold nanorod-functionalised titanium is that the titanium substrate dampens the localised surface plasmons of the gold nanorods. It has been shown that chemical interface plasmon damping can occur for lithographically fabricated gold nanorods on top of a titanium adhesion layer [27]. Even though the gold nanorods it this project are chemisorbed onto a titanium dioxide layer on top of the titanium substrate, it is possible that a similar plasmon damping phenomena could occur.

4.3.2.1 Bacterial morphology study

When visualising the surfaces from the microbiology study on the gold nanorod-functionalised titanium, no evident difference in the morphology of the *S. epidermidis* could be noticed between the test groups. This was expected as no antimicrobial activity could be observed during the *in vitro* study. When comparing the untreated and the post-treated gold nanorod-functionalised titanium it was noted that there seemed to have been an larger amount of gold nanorods detached from the untreated titanium surfaces compared to the post-treated one. As shown by the SEM micrographs (75 000x magnification) in Figure 4.11, some of the bacteria on the untreated gold nanorod-functionalised titanium were covered in gold nanorods that had detached from the surface, while this phenomena was not noticed to the same extent for the post-treated sample. These findings give further evidence that the post-treatment causes a sintering of the gold nanorods to occur and improve their attachment to the titanium substrate, as previously discussed in section 4.2.3.

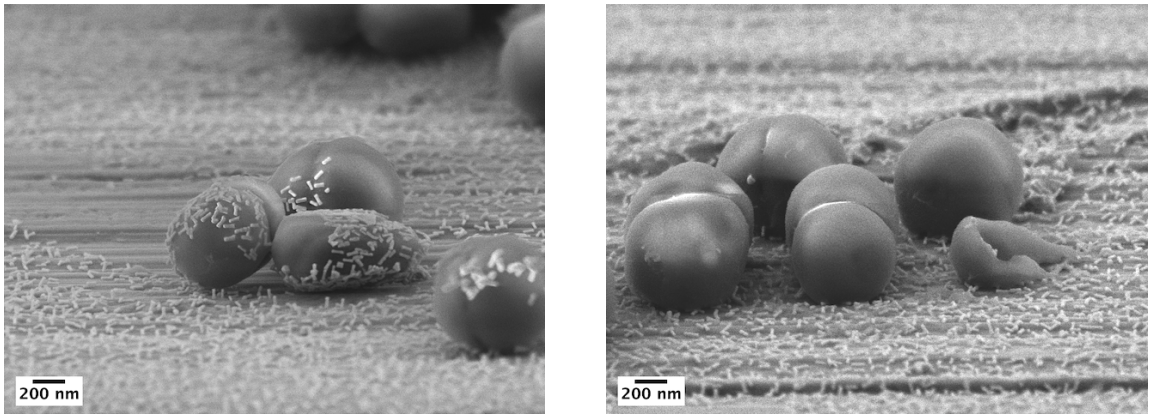

(a) Untreated **(b)** Post-treated

Figure 4.11: SEM micrographs at 75 000x magnification of *S. epidermidis* on untreated and post-treated gold nanorod-functionalised titanium.

4.3.3 Gold nanorod 700 nm-functionalised titanium

The *in vitro* study with gold nanorods 700 nm assembled onto titanium was conducted to evaluate whether the lack of antimicrobial activity observed for the gold nanorod-functionalised titanium surfaces could be due to a shift of the LSPR frequency occurring for the gold nanorods once attached to a titanium substrate. The gold nanorod

700 nm-functionalised titanium surfaces used in the microbiology study had a surface coverage of 17-21%, corresponding to 226-280 gold nanorods 700 nm/μm^2. As shown by the representative fluorescence images in Figure 4.12, no obvious difference in the amount of dead (red) and live (green) bacteria could be noticed between the three test groups.

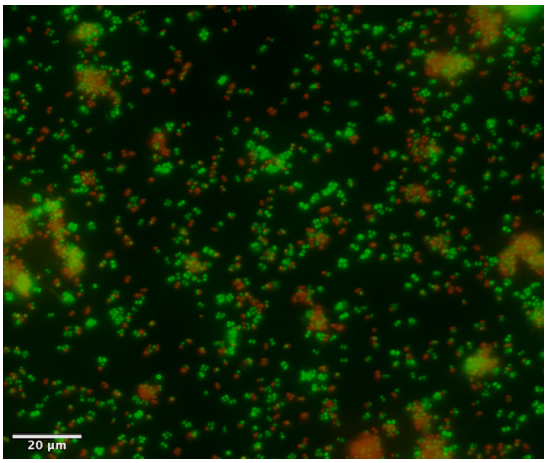

(a) Ti + NIR

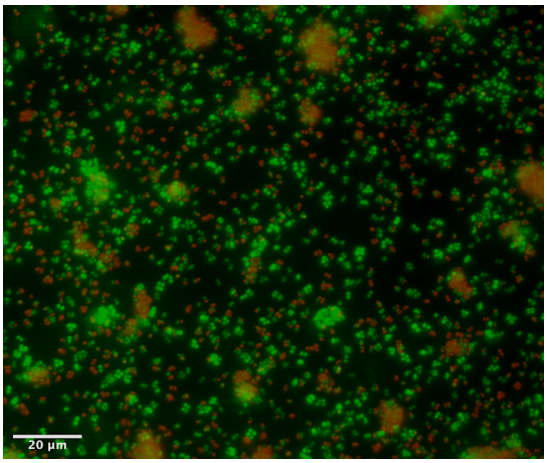

(b) TiAuNR700

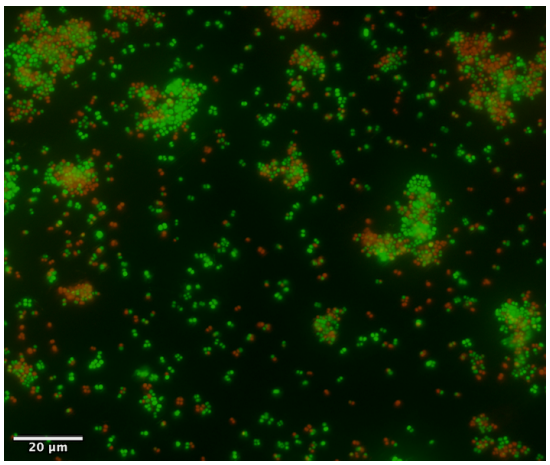

(c) TiAuNR700 + NIR

Figure 4.12: Images from fluorescence microscopy of samples after LIVE/DEAD™ staining from the *in vitro* study with *S. epidermidis* on gold nanorod 700 nm-functionalised titanium.

The result from the image analysis of the fluorescence micrographs for all three replicates, determining the average percentage of dead bacteria on the surfaces, is presented in Figure 4.13. For the bare titanium irradiated with NIR light for 5 min (Ti + NIR) the average percentage of dead cells was 49%, for the gold nanorod 700 nm-functionalised titanium (TiAuNR700) it was 47%, and for the gold nanorods 700 nm-functionalised titanium irradiated with NIR for 5 min (TiAuNR700 + NIR) it was 58 %. When performing a Wilcoxon rank sum test with a significance level of 1% on the data from the image analysis, no significant difference could be shown between

the percentage of dead bacteria on the TiAuNR700 + NIR compared to each of the control groups.

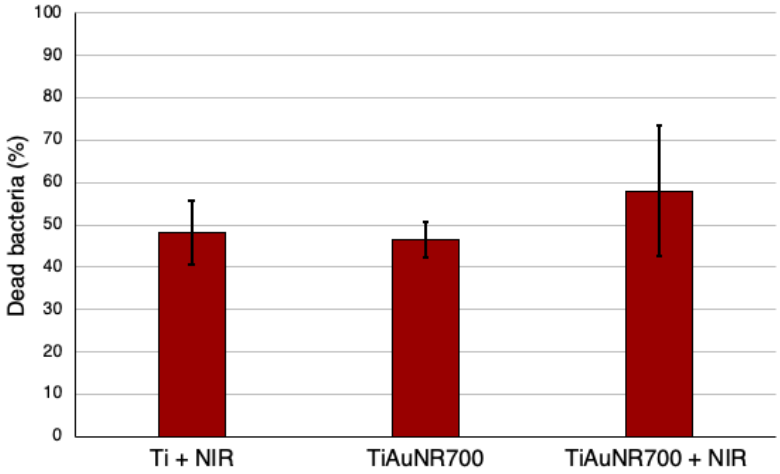

Figure 4.13: Percentage of dead bacteria covering the surfaces from the *in vitro* study with *S. epidermidis* on gold nanorod 700 nm-functionalised titanium.

The average percentage of dead bacteria was slightly higher for TiAuNR700 + NIR, but as indicated by the large standard deviation for that test group in Figure 4.13, the percentage varied a lot between the three replicates. In Table 4.3 the percentage of dead cells for each replicate of each test group is presented. Replicate 2 for TiAuNR700 + NIR had almost 80% dead bacterial cells, while all other replicates for all test groups in general had between 45-55% dead cells. The rather deviating result for replicate 2 of TiAuNR700 + NIR could be due to that sample being contaminated during the study. A possible contamination source could be the tweezers used to move the titanium discs during the procedure. The tweezers were sterilised with 70% ethanol to avoid cross-contamination between the samples. If some ethanol remained on the tweezers and was transferred to the sample, this could explain the higher percentage of dead cells observed for that replicate. All in all, the results from the microbiology study could not show any significant antimicrobial activity being achieved upon NIR irradiation of the gold nanorod 700 nm-functionalised titanium.

	Average percentage of dead cells (%)		
	Ti + NIR	**TiAuNR700**	**TiAuNR700 + NIR**
Replicate 1	42 ± 5.0	43 ± 2.0	47 ± 2.3
Replicate 2	45 ± 2.5	46 ± 3.4	79 ± 2.8
Replicate 3	57 ± 3.9	50 ± 1.7	49 ± 3.5

Table 4.3: Percentage of dead cells on the surfaces for each replicate from the *in vitro* study on gold nanorod 700 nm-functionalised titanium.

The results from the *in vitro* study using the gold nanorods with a longitudinal LSPR frequency at 700 nm give an indication that a shift in the resonance frequency, as

discussed in Section 4.3.2, is likely not the only reason as to why no antimicrobial activity could be observed for the titanium functionalised with the gold nanorods with a resonance frequency at 850 nm. A shift in the resonance frequency should occur upon attachment of the gold nanorods to the titanium substrate as the refractive index changes drastically compared to the nanorods in aqueous dispersion, but this shift is probably not the only or the predominant reason causing the lack of antimicrobial activity. The second possibility mentioned in Section 4.3.2, i.e. that the titanium substrate has a plasmon damping effect on the gold nanorods, is with high probability also a major contributing factor.

A possible way to reduce the plasmon damping, which was not evaluated due to time constraints, could be by increasing the thickness of the titanium dioxide layer covering the titanium substrate. It has been shown that the use of a less absorptive material such as TiO_2 reduces the damping, as the disruption of the plasmon resonance stems from the real and imaginary parts of the adhesion materials dielectric function that influence the refractive index and introduces absorption [28]. Likewise, by coating the titanium in another biocompatible and less absorptive material before the gold nanorod surface assembly, a reduction of the plasmon damping may be attained. By achieving a reduced plasmon damping, and combining it with tuning of the gold nanorod dimensions depending on the LSPR frequency shift occurring once assembled on titanium, it is likely that an antimicrobial activity, as observed for the gold nanorod-functionalised glass, could be obtained.

4.3.4 Gold nanorod toxicity

For all three *in vitro* studies with the gold nanorod-functionalised surfaces, no significant difference in the amount of dead bacteria was observed for the bare glass respectively titanium and the non-irradiated gold nanorod-functionalised glass respectively titanium. In each study the two control groups exhibited similar amounts of dead cells, indicating that the gold nanorods themselves do not seem to have a toxic effect on the *S. epidermidis*. It is likely that the CTAB remaining on the surface assembled gold nanorods is at such low concentrations that no toxic effect is caused on the bacteria. By also including the post-treatment, that showed strong indications of being efficient in removing the remaining CTAB as mentioned in Section 4.2.3, the risk of the gold nanorods inducing toxicity could be further minimised. All together, these observations show promise for potential future biological applications.

5

Conclusion

By using gold nanorod-functionalised surfaces that are exposed to near-infrared light of the nanorods' localised surface plasmon resonance frequency, photothermal elimination of bacteria growing on the surfaces can be achieved. In the project gold nanorods of two different aspect ratios have been synthesised. The gold nanorods with an aspect ratio of 3.4 exhibited a longitudinal absorption band in the near-infrared region at 850 nm, while the smaller nanorods with an aspect ratio of 2.6 had a longitudinal band at 700 nm. The photothermal effect of the gold nanorods causing a local heating, due to the decay of localised surface plasmons, was demonstrated by a temperature increase measured upon irradiation of an aqueous dispersion of gold nanorods with NIR light.

A procedure for the surface assembly of gold nanorods, wherein the nanorods are chemisorbed onto both titanium and glass substrates via (3-mercaptopropyl)trimethoxysilane as a linker, was developed. The gold nanorod-functionalised glass surfaces exhibited a lower surface coverage of nanorods compared to the titanium surfaces, which was attributed to differences in surface chemistry och roughness between the two materials. The surface coverage of gold nanorods on titanium was shown to increase with immersion time in gold nanorod dispersion in Milli-Q, and appeared to reach a saturated state around 20% coverage. The surface coverage achieved was deemed suitable for the aimed application, as a too high coverage of gold nanorods could impede on the integration properties of the titanium implant.

The post-treatment of the gold nanorod-functionalised titanium showed clear indications of being successful both in improving the surface attachment between the gold nanorods and the titanium substrate through sintering of the nanorods, as well as in removing remaining CTAB from the nanorods. Future investigations with more mechanical testing of the surface attachment of the gold nanorods would be of interest in order to ensure that detachment of the nanorods upon implantation is prevented.

From the *in vitro* study with *S. epidermidis* performed on the gold nanorod-functionalised glass, an evident antimicrobial activity could be observed upon irradiation with NIR light. Between 40-50% more dead bacteria was observed on the gold nanorod-functionalised glass irradiated with NIR light compared to the control groups. A more prominent effect could have been achieved if the study was repeated with glass surfaces with a higher coverage of gold nanorods, exposing each bacteria to a larger number of nanorods. The results show that the principle of using gold nanorods attached to a surface that is irradiated with NIR light in order to photothermally

eliminate bacteria from the surface is valid and shows promise to help in the fight against implant-associated infections.

The two *in vitro* studies performed with *S. epidermidis* on titanium surfaces functionalised with gold nanorods and gold nanorod 700 nm, respectively, did not show any antimicrobial activity being achieved upon irradiation with NIR light. The lack of antimicrobial activity observed was attributed to two main factors; a red-shift occurring in the LSPR frequency of the gold nanorods due to changes in refractive index arising once assembled on the titanium substrate, and the titanium substrate having a plasmon damping effect on the gold nanorods. The plasmon damping caused by the titanium substrate was reasoned to be the predominant cause as there could be no increase in bacterial elimination observed for the gold nanorod 700 nm-functionalised titanium compared to the gold nanorod-functionalised titanium. A great prospect would be to modify the surface of the titanium substrate by either increasing the titanium dioxide thickness, or by coating with another biocompatible and less absorptive material, as this could reduce the plasmon damping effect. By modifying the titanium surface before attaching the gold nanorods and thereby minimise potential plasmon damping, and combining this with tuning of the gold nanorod dimensions depending on the LSPR frequency shift occurring, it could be possible to achieve the aimed for photothermal elimination of bacteria upon NIR irradiation on gold nanorod-functionalised titanium as well as on glass.

Throughout all three microbiology studies performed, no evident increase in dead bacteria caused by the gold nanorods themselves could be observed. By complementing with the post-treatment in order to minimise the risk of toxicity by removing the remaining CTAB from the nanorods, the lack of toxicity observed shows potential for future biological applications. A next step would be performing co-culture investigations to evaluate the effect of the gold nanorod-functionalised surfaces that are exposed to NIR light on tissue cells along with bacterial cells. It would be of great interest and importance for future applications to assess how tissue cells are affected by the gold nanorods and the heat generated by the nanorods upon irradiation with NIR light.

Bibliography

[1] Darouiche RO. Treatment of Infections Associated with Surgical Implants. The New England Journal of Medicine. 2004;350(14):1422–1429.

[2] Hetrick EM, Schoenfisch MH. Reducing implant-related infections: active release strategies. Chemical Society Reviews. 2006;35(9):780–789.

[3] Arciola CR, Campoccia D, Montanaro L. Implant infections: adhesion, biofilm formation and immune evasion. Nature Reviews Microbiology. 2018;16:397–409.

[4] Høiby N, Bjarnsholt T, Givskog M, Molin S, Ciofu O. Antibiotic resistance of bacterial biofilms. International Journal of Antimicrobial Agents. 2010;35(4):322–332.

[5] The European Centre for Disease Prevention and Control. Surveillance of antimicrobial resistance in Europe 2018. ECDC; 2019.

[6] Murphy CJ, Alkilany AM, Thompson LB, Boulos SP, Sisco PN. Gold nanorods: Their potential for photothermal therapeutics and drug delivery, tempered by the complexity of their biological interactions. Advanced Drug Delivery Reviews. 2012;64(2):190–199.

[7] Pihl M, Bruzell E, Andersson M. Bacterial biofilm elimination using gold nanorod localised surface plasmon resonance generated heat. Materials Science and Engineering: C. 2017;80:54–58.

[8] Kaur M, Singh K. Review on titanium and titanium based alloys as biomaterials for orthopaedic applications. Materials Science and Engineering: C. 2019;102:844–862.

[9] Tapscott DC, Wottowa C. Orthopedic Implant Materials. Treasure Island, Florida: StatPearls Publishing; 2020.

[10] Scarabelli L, Sánchez-Iglesias A, Pérez-Juste J, Liz-Marzán LM. A "tips and tricks" Practical Guide to the Synthesis of Gold Nanorods. The Journal of Physical Chemistry Letters. 2015;6(21):4270–4279.

[11] Huang X, Neretina S, El-Sayed MA. Gold Nanorods: From Synthesis and Properties to Biological and Biomedical Applications. Advanced Materials. 2009;21(48):4880–4910.

[12] Kelly KL, Coronado E, Zao LL, Scatz GC. Optical Properties of Metal Nanoparticles: The Influence of Size, Shape, and Dielectric Environment. The Journal

of Physical Chemistry B. 2003;107(3):668–677.

[13] Mayer KM, Hafner JH. Localized Surface Plasmon Resonance Sensors. Chemical Reviews. 2011;111(6):3828–3857.

[14] El-Sayed MA. Some Interesting Properties of Metals Confined in Time and Nanometer Space of Different Shapes. Accounts of Chemical Research. 2001;34(4):257–264.

[15] Nikoobakht B, El-Sayed MA. Preparation and Growth Mechanism of Gold Nanorods (NRs) Using Seed-Mediated Growth Method. Chemistry of Materials. 2003;15(10):1957–1962.

[16] Vigderman L, Khanal BP, Zubarev ER. Functional Gold Nanorods: Synthesis, Self-Assembly, and Sensing Applications. Advanced Materials. 2012;24(36):4811–48412.

[17] Alkilany AM, Murphy CJ. Toxicity and cellular uptake of gold nanoparticles: what we have learned so far? Journal of Nanoparticle Research. 2010;12(7):2313–2333.

[18] Connor EE, Mwamuka J, Gole A, Murphy CJ, Wyatt MD. Gold Nanoparticles Are Taken Up by Human Cells but Do Not Cause Acute Cytotoxicity. Small. 2005;1(3):325–327.

[19] Marinakos SM, Chen S, Chilkoti A. Plasmonic Detection of a Model Analyte in Serum by a Gold Nanorod Sensor. Analytical Chemistry. 2007;79(14):5278–5283.

[20] Owen T. Fundamentals of modern UV-visible spectroscopy: Primer. Agilent Technologies; 2000.

[21] Egerton RF. Physical Principles of Electron Microscopy. Boston, Massachusetts: Springer; 2005.

[22] Lindon JC, Koppenaal DW, Tranter GE. Encyclopedia of Spectroscopy and Spectrometry. Elsevier Science & Technology; 2016.

[23] Lichtman JW, Conchello JA. Fluorescence microscopy. Nature Methods. 2005;2(12):910–919.

[24] Invitrogen Molecular Probes. LIVE/DEAD BacLight Bacterial Viability Kits. ThermoFischer Scientific; 2004.

[25] Funston AM, Novo C, Davis TJ, Mulvaney P. Plasmon Coupling of Gold Nanorods at Short Distances and in Different Geometries. Nano Letters. 2009;9(4):1651–1658.

[26] Rumble JR, editor. Handbook of Chemistry and Physics Online. CRC Press; 2020.

[27] Habteyes TG, Dhuey S, Wood E, Gargas D, Cabrini S, Schuck PJ, et al. Metallic Adhesion Layer Induced Plasmon Damping and Molecular Linker as a Nondamping Alternative. ACS Nano. 2012;6(6):5702–5709.

[28] Siegfried T, Ekinci Y, Martin OJF, Sigg H. Engineering Metal Adhesion Layers That Do Not Deteriorate Plasmon Resonances. ACS Nano. 2013;7(3):2751–2757.

A

Appendix

A.1 Calculation of the concentration of gold nanorod dispersions

The concentrations of the gold nanorod dispersions used in the project were derived from the measured absorbance of the dispersions at 400 nm. The concentrations derived from the absorbance were compared with concentrations from theoretical calculations based on the synthesis procedure.

A.1.1 Concentration from UV-Vis-NIR spectroscopy

From the average absorbance, A, at 400 nm of a gold nanorod dispersion, the concentration of Au(0) in the dispersion can be calculated as

$$[Au(0)] = \frac{A}{1.2} * 0.5mM$$

Based on that an absorbance of 1.2 at 400 nm corresponds to [Au(0)]=0.5 mM [10]. The amount of Au(0) in moles can then be calculated by knowing the total volume, V, of the dispersion of gold nanorods.

$$n_{Au(0)} = [Au(0)] * V$$

The amount of Au(0) in moles can thereafter be expressed as a volume.

$$V_{Au(0)} = \frac{n_{Au(0)} * M_{Au(0)}}{\rho_{Au(0)}}$$

From the average dimensions of the gold nanorods, determined by image analysis of SEM micrographs, the volume of a nanorod can be calculated by estimating it with the volume of a cylinder.

$$V_{nanorod} = \pi * l * (\frac{w}{2})^2$$

Where l is the length of the nanorod and w the width. Thereafter, the amount of nanorods in moles can be calculated.

$$n_{nanorod} = \frac{V_{Au(0)}}{V_{nanorod} * N_A}$$

Lastly, the concentration of gold nanorods is calculated by dividing with the total volume of the nanorod dispersion.

$$[nanorod] = \frac{n_{nanorod}}{V}$$

A.1.2 Concentration from theoretical calculations

In the seed solution, the total amount of Au(III) added from the gold(III) chloride trihydrate is

$$n^{seed}_{Au(III)} = 25 * 10^{-6}l * 50 * 10^{-3}M = 1.25 * 10^{-6}mole$$

By knowing the total volume of the seed solution, V^{seed}_{tot}, and assuming that 95% of the added Au(III) is reduced to Au(0), the concentration of Au(0) in the seed solution can be determined.

$$[Au(0)]_{seed} = 0.95 * \frac{n^{seed}_{Au(III)}}{V^{seed}_{tot}} = 0.95 * \frac{1.25 * 10^{-6}mole}{5.025 * 10^{-3}l} = 2.36 * 10^{-4}M$$

As 24 μl of the seed solution is added to the growth solution, the amount Au(0) in mole added from the seed is

$$n^{seed}_{Au(0)} = 24 * 10^{-6}l * 2.36 * 10^{-4}M = 5.67 * 10^{-9}mole$$

By knowing the amount of gold(III) chloride trihydrate added to the growth solution and assuming that 95% of the added Au(III) is reduced to Au(0), the amount of Au(0) in moles in the growth solution can be calculated.

$$n^{growth}_{Au(0)} = 0.95 * 100 * 10^{-6}l * 50 * 10^{-3}M = 4.75 * 10^{-6}mole$$

The total amount of Au(0) in the synthesis is thus

$$n_{Au(0)} = n^{seed}_{Au(0)} + n^{growth}_{Au(0)} = 4.75567 * 10^{-6}mole$$

The total volume of Au(0) can then be determined.

$$V_{Au(0)} = \frac{n_{Au(0)} * M_{Au(0)}}{\rho_{Au(0)}} = \frac{4.75567 * 10^{-6}mole * 196.97g/mole}{19.3 * 10^{6}g/m^3} = 4.85 * 10^{-11}m^3$$

Through knowing the average dimensions of the gold nanorods, the amount of nanorods in moles can then be determined.

$$n_{nanorod} = \frac{V_{Au(0)}}{V_{nanorod} * N_A}$$

The theoretical concentration of gold nanorods in the produced nanorod dispersion can thereafter be determined by diving with the total volume of the dispersion, V, which is determined by the amount of Milli-Q water used to redisperse the nanorods after the final centrifugation.

$$[nanorods] = \frac{n_{nanorod}}{V}$$

A.2 SEM micrographs of gold nanorod-functionalised titanium

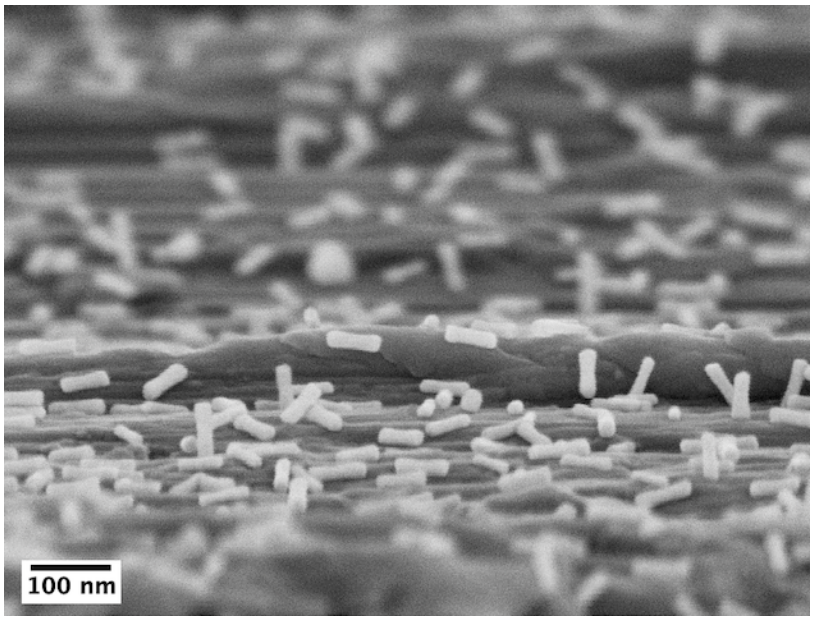

Figure A.1: SEM micrograph at 250 000x magnification showing a side view of gold nanorods surface assembled on titanium

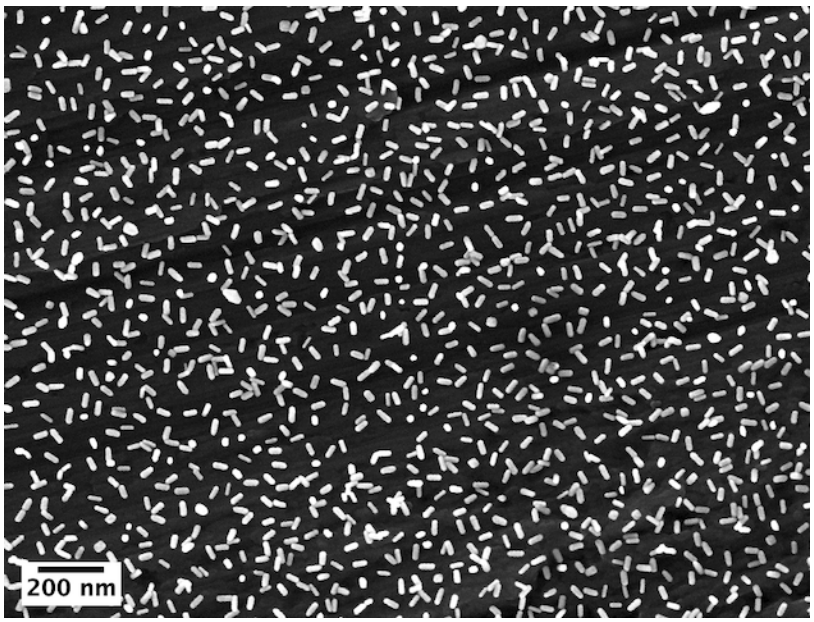

Figure A.2: SEM micrograph at 100 000x magnification of gold nanorods 700 nm surface assembled on titanium

A.3 X-ray photoelectron spectroscopy survey spectra

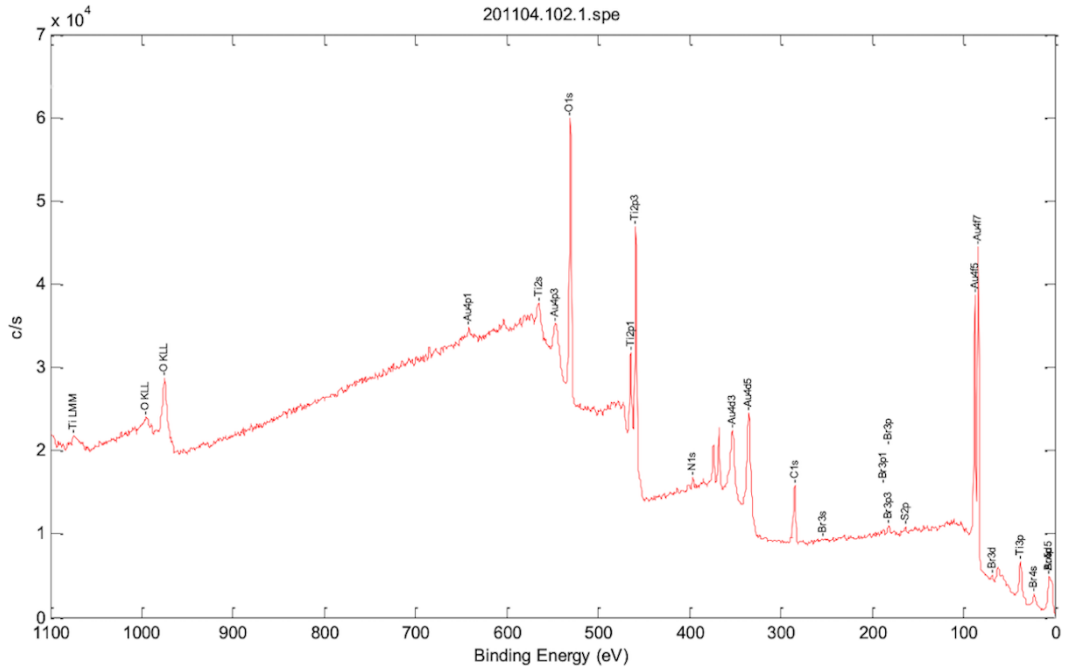

Figure A.3: X-ray photoelectron spectroscopy survey spectrum for gold nanorod-functionalised titanium

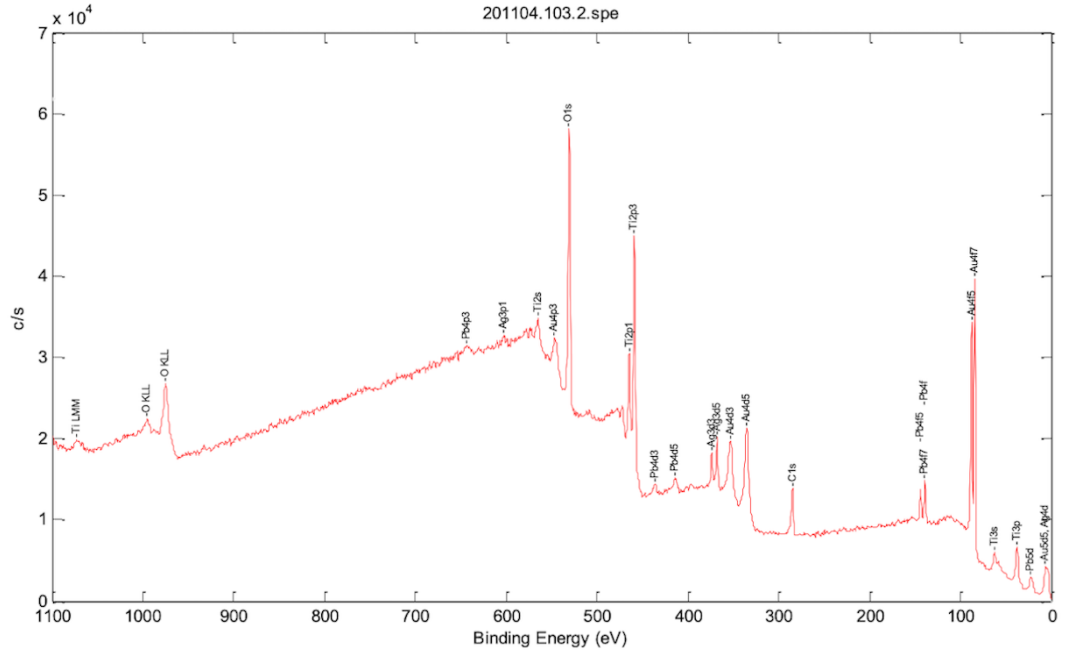

Figure A.4: X-ray photoelectron spectroscopy survey spectrum for gold nanorod-functionalised titanium post-treated with heat and oxygen plasma